corrected the abnormal down-regulation of PKC in cells from beige mice and CHS patients. In addition, these inhibitors corrected other cellular abnormalities such as giant granule formation in fibroblasts, decreased lysosomal enzyme activity, defective NK activity and abnormally increased Con A cap formation in beige mice [11–14].

Recently we reported that E-64-d administration to beige mice either orally or intraperitoneally for three consecutive days (12.5 mg/kg body weight per day), reverses the abnormally increased Con A cap formation, decreased lysosomal enzyme activity, and the delayed bactericidal activity against *S. aureus* in PMNs isolated from beige mice [15]. We also demonstrated that administration of E-64-d to beige mice decreases their susceptibility to *S. aureus* infections. These findings suggest that administration of E-64-d may be effective for preventing severe bacterial infections in human CHS patients.

We previously showed that E-64-d reverses the increased Con A cap formation and the decreased lysosomal enzyme activity in EB virus-transformed CHS cell lines *in vitro* [16]. However, the effects of E-64-d on the compromised NK and bactericidal activities responsible for the severe microbial infections observed in human CHS patients have not been clarified. We therefore examined whether E-64-d could reverse the decreased NK and delayed bactericidal activities against *S. aureus* mediated by peripheral blood leukocytes isolated from six Japanese CHS patients *in vitro*.

2. Materials and methods

2.1. Patients

Peripheral blood samples were obtained from six CHS patients who had not undergone bone marrow transplantation. We examined two males, four females, and five normal healthy individuals (controls). The study was performed when all the patients were free of infection. Informed consent was obtained from the patients or their families for this study, and the study protocol was approved by the Ethics Committee of the University of Yamanashi.

2.2. Reagents

E-64-d [ethyl (+)-(2S, 3S)-3-[(S)-3-methyl-1-(3-methylbutylcarbamoyl) butyl-carbamoyl]-2-oxiranecarboxylate] used in this study was kindly provided by Taisho Pharmaceutical Co. (Saitama, Japan). Hanks' balanced salt solution (HBSS) and phosphate-buffered saline (PBS) were from Invitrogen Co. (Carlsbad, CA, USA). The [γ-^{32}p] ATP and the PKC enzyme assay system were purchased from GE Healthcare Bio-Science Co. (Piscataway, NJ, USA). Chromium-51 radionuclide was obtained from PerkinElmer Japan Co. (Yokohama, Japan). Chelerythrin and GÖ6976 were from Merck (Darmstadt, Germany). Lysostaphin and other chemicals were purchased from Sigma Chemical Co. (St Louis, MO, USA). SCD agar and heart infusion broth were obtained from Eiken Chemical Co. (Tokyo, Japan).

2.3. Bacteria

A coagulase-positive, methicillin-sensitive and vancomycin-sensitive strain of *S. aureus*, which was isolated from the University of Yamanashi Hospital, was used in this study. Bacteria were grown for 12 h in heart infusion broth at 37 °C. Subsequently, the bacterial culture was kept at 4 °C until further use. Serial 10-fold dilutions were made from this bacterial culture and these were plated on SCD agar plates. After an overnight culture, the colonies were counted and the bacterial culture was diluted to the desired concentrations.

2.4. Separation of peripheral blood mononuclear cells (PBMCs) and PMNs

PBMCs and PMNs from patients and normal controls were isolated using the monopoly resolving medium (Dainippon Sumitomo Pharma Co., Osaka, Japan) according to the manufacturer's protocol. The isolated PBMCs were washed three times and suspended in RPMI 1640 with 10% FBS, and PMNs were washed and suspended in Hanks' balanced salt solution. The PMNs obtained were 90–94% pure as determined by May-Giemsa staining: the remainder was lymphocytes and monocytes. The viability of these cells was more than 95% as assessed by trypan blue exclusion.

2.5. NK assay

Cells from the human erythroleukemia cell line, K562, were used as targets for evaluating NK activity. One million of these target cells were labeled with 100 μCi of chromium-51 radionuclide for 1 h at 37 °C. These were then washed three times with RPMI 1640 plus 10% FBS. Effector cells were suspended in 200 μl RPMI 1640 with 10% FBS in each well of a microplate (Nunclon Delta, Nunc). E-64-d or other reagents were added to the cells and incubated for 1 h at 37 °C. Then, 1×10^4 labeled target cells were added to the mixture at an effector: target cell ratio of 40:1. The microplates were incubated at 37 °C in a 5% CO_2 atmosphere for 4 h. After this incubation, 100 μl of the cultured supernatant was collected and the radioactivity was measured. The percent cytotoxicity was calculated according to the following formula:

$$\text{Percent cytotoxicity} = (\text{experimental release} - \text{spontaneous release} / \text{maximum release} - \text{spontaneous release}) \times 100.$$

Spontaneous release was assessed by incubating target cells with medium alone. The maximum release was determined by mixing target cells with 1 N NaOH. All assays were run in triplicate.

2.6. Bactericidal assays

Bactericidal assays were performed according to the method described by Gallin et al. [17]. For these studies, 5×10^6 PMNs were suspended in HBSS with 10% fresh normal human serum, and were incubated at 37 °C for 10 min before adding 5×10^7 bacteria. In some cases, the cells were incubated with E-64-d for 30 min, before normal human serum was added. The PMN suspension was then tumbled for 20 min to allow phagocytosis to occur. Then, lysostaphin (final concentration 10 U/ml), which kills extracellular bacteria, was added and the tumbling was continued. Samples (0.1 ml) were obtained at 30-, 60-, and 90-min intervals. These were washed three times with ice-cold HBSS, and then placed in 1 ml of distilled water to rupture the cells for total viable bacterial counts. Serial 10-fold dilutions were made and plated onto SCD agar plates. After an overnight culture at 37 °C, the number of colonies was counted.

2.7. Assay for PKC activity

After PBMCs were treated with E-64-d or stimulated with Con A, cells (3×10^6) were disrupted by sonication for 10 s three times at 4 °C in 20 mM Tris–HCl (pH7.5), 0.25 M sucrose, 2 mM EDTA, 5 mM EGTA, 2 mM phenylmethylsulfonylfluoride, 0.01% leupeptin, and 50 mM 2-mercaptoethanol. The cytosolic and membrane fractions were prepared as described previously [10]. PKC activity was assayed by using a PKC enzyme assay system (GE Healthcare Bio-Science Co.) according to the manufacturer's protocol.

2.8. Statistics

All experiments were repeated at least two times. Statistical analyses were performed using a standard Student's *t*-test.

3. Results

3.1. E-64-d reverses the deficient NK activity of PBMCs isolated from CHS patients

We began by examining the NK activity of PBMCs isolated from six CHS patients. As shown in Fig. 1, the mean NK activity against K562 cells measured from the cells of these CHS patients ($n=6$) was significantly lower than that of normal controls ($n=5$; $p<0.01$). We next examined the effect of E-64-d on NK activity. E-64-d is a membrane-permeable analogue of E-64-c, and Ki of E-64-c for calpain is 0.33 μg/ml (0.96 μM) [16]. When the cells were incubated with E-64-d (1 μg/ml: 2.92 μM) for 1 h, NK activity was significantly enhanced ($p<0.01$). This dose of E64-d did not affect the NK activity of normal controls.

3.2. E-64-d restores the delayed bactericidal activity of PMNs isolated from CHS patients

It is known that the leukocytes from CHS patients exhibit delayed bactericidal activity against gram-positive bacteria including *S. aureus*. We therefore examined whether E-64-d improved the *in vitro* bactericidal activity of PMNs isolated from CHS patients against *S. aureus*. The relative amounts of isolated PMNs from CHS patients and normal controls were 54.2–70.8% and 62.2–75.4%, respectively. As shown in Table 1, bactericidal activity of PMNs from CHS patients was significantly lower than that observed in normal controls at 30-, 60-, and 90-min intervals. Incubation of PMNs with E-64-d (1 μg/ml) for 30 min, however, restored the bactericidal activity to almost normal levels. In contrast, this dose of E64-d did not significantly alter the bactericidal activity of normal controls.

3.3. E-64-d eliminates the abnormal down-regulation of PKC in Con A-stimulated PBMCs isolated from CHS patients

We previously reported that the membrane-bound PKC activity in CHS cells is abnormally down-regulated after Con A-stimulation [13,14]. Therefore we examined whether the E-64-d-mediated improvement of NK and bactericidal activity was associated with an elimination of this down-regulated PKC activity in PBMCs from CHS patients. In normal cells, membrane-bound PKC activity increased after 20-min of Con A-stimulation (Fig. 2A), while cytosolic enzyme activity decreased (Fig. 2B). In contrast, the membrane-bound PKC activity in CHS cells drastically decreased following Con A-stimulation (Fig. 2B). E-64-d (1 μg/ml) reversed this decline of membrane-bound PKC activity in CHS cells (Fig. 2). The PKC activity of normal cells was not significantly altered by the same dose of E-64-d.

Table 1
Effect of E-64-d on the bactericidal activity of PMNs isolated from CHS patients

	Treatment	Bactericidal activity (% *S. aureus* killed)		
		30 min	60 min	90 min
Normal	Medium	40.54±1.49	66.75±2.52	90.24±0.55
	E-64-d	39.88±0.82	65.98±3.92	91.65±1.1
CHS	Medium	23.57±0.72*	54.3±2.08**	81.6±1.44**
	E-64-d	36.15±0.81	64.47±1.42	88.33±0.77

The PMNs from CHS ($n=6$) and normal controls ($n=5$) were incubated with E-64-d (1 μg/ml) or medium alone for 30 min. Then the bactericidal activity against *S. aureus* was examined as described in "Materials and methods". Data represent the mean±SE.
*$p<0.01$, **$p<0.05$, significant when compared with normal control and E-64-d-treated CHS.

3.4. PKC inhibitors suppress both NK and bactericidal activities of normal leukocytes

To examine whether NK and bactericidal activities are associated with PKC activity, we tested the effects of two potent PKC inhibitors, chelerythrin and GÖ6976. It is known that chelerythrin inhibits PKC activity by blocking the catalytic domain of PKC (IC50=660 nM) [18]. GÖ6976 selectively inhibits Ca^{2+}-dependent PKC isozymes, including PKC α (IC50=2.3 nM) and β_1 (IC50=6.2 nM) [19].

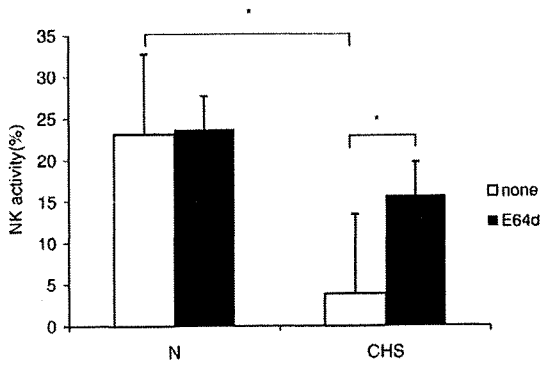

Fig. 1. Effect of E-64-d on the NK activity of CHS patients. After PBMC from CHS patients ($n=6$) and normal control ($n=5$) were incubated with E-64-d (1 μg/ml) or medium alone for 1 h, a NK activity against K562 cells was assayed as described in 'Materials and methods'. The data represent the mean±SE of each group. *$p<0.01$.

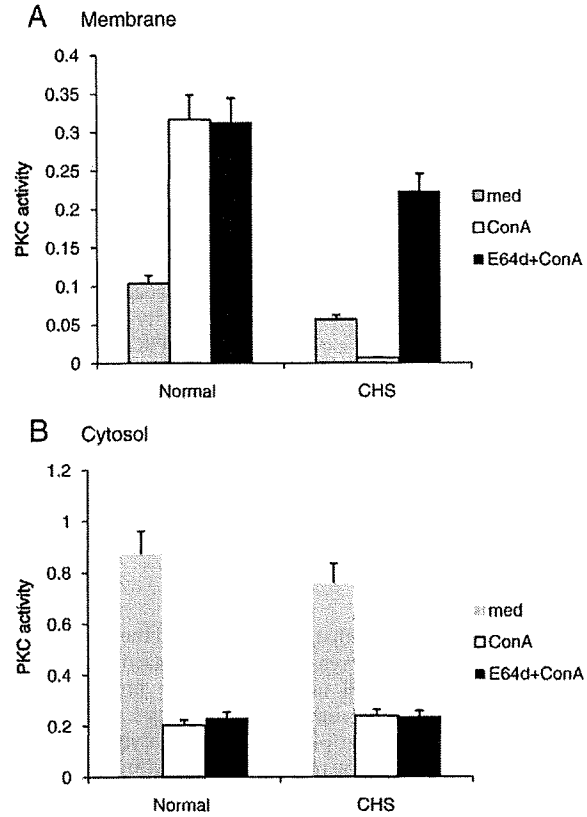

Fig. 2. Effect of E-64-d on the PKC activity of Con A-stimulated PBMCs isolated from CHS patients. PBMCs from CHS patients and normal controls were incubated with E-64-d (1 μg/ml) or medium alone for 1 h. Then the cells were stimulated with or without Con A (20 μg/ml) for 20 min. Membrane-bound (A) and cytosolic (B) PKC activity was assayed as described in "Materials and methods". The data represent the mean (pmol/min/10^7 cells) of three patients and normal controls. The data represent the mean±SE.

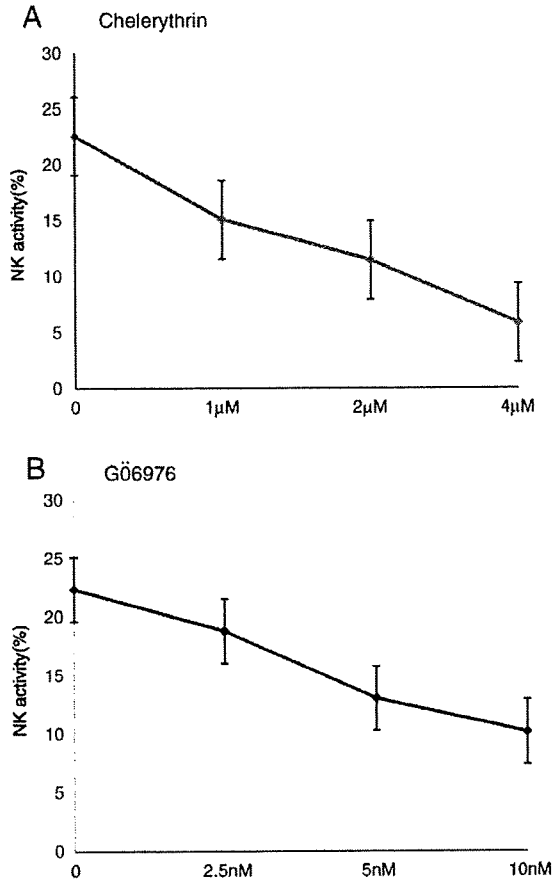

Fig. 3. Effect of potent inhibitors of PKC on normal NK activity. After PBMCs isolated from normal controls were incubated with various doses of either chelerythrin (A) or GÖ6976 (B) for 30 min, a NK assay was performed as described in "Materials and methods". The data represent the mean±SE of three experiments.

The data presented in Fig. 3A indicated that chelerythrin inhibited the NK activity of normal PBMCs in a dose-dependent manner. In addition, GÖ6976 significantly inhibited NK activity at doses known to inhibit Ca^{2+}-dependent PKC isozymes including PKCα and β_1 (Fig. 3B). These results suggested that at the very least the conventional PKC isozymes are related to the deficiency of NK activity in CHS.

As shown in Table 2, both chelerythrin (2 μM) and GÖ6976 (10 nM) significantly inhibited the bactericidal activity of normal PMNs against *S. aureus* at 30, 60, and 90 min. These data suggested that a decline in PKC activity is responsible for the deficiency in both NK and bactericidal activities in CHS patients.

4. Discussion

We previously reported that E-64-d corrected the abnormal Con A cap formation and the decreased lysosomal enzyme activity in EB virus-transformed CHS cell lines [16]. In the present study, we demonstrated for the first time that deficiencies in both NK and bactericidal activities of peripheral blood leukocytes isolated from CHS patients are improved by treating the cells with E-64-d *in vitro*. It is known that NK cells play critical roles in defense against tumor cell growth and viral infection. CHS patients often die due to the severe infections by gram-positive bacteria or lymphoproliferative disorders. Therefore, the preservation of NK and the bactericidal activities may be critical for CHS patients.

Root et al. [20] reported that CHS leukocytes can normally ingest of a variety of bacteria including *S. aureus*. After phagocytosis, CHS granulocytes exhibit a normal burst in oxygen consumption. In their report, the greatest defect in the killing ratio was observed 20 min following the initial contact of CHS cells with the bacteria. The CHS cells had enlarged granules, which failed to efficiently fuse with the cell membrane. Although the oxidative burst was normal, the delivery of peroxidase to many phagosomes did not occur [20]. In addition, lysosomal elastase and cathepsin G activities were selectively impaired in the CHS cells [21]. This deficient lysosomal enzyme activity may cause CHS patients to be highly susceptible to a variety of infections. These two lysosomal enzymes reportedly undergo similar processing in the Golgi apparatus [22]. We previously showed that PKC inhibitors suppress these two enzyme activities in normal murine fibroblasts [12]. Therefore, it is possible that PKC is involved in the generation of the active form of elastase and cathepsin G by some unknown mechanism. In addition, we reported that PKC is involved in giant granule formation [12]. The present study findings indicated that E-64-d may improve the delivery of peroxidase and lysosomal enzymes.

We and other researchers have demonstrated that the activation of PKC plays a major role in the lytic system of NK cells [23,24]. After receptor recognition of target cells, a subsequent Ca^{2+}-dependent exocytosis of lytic granules occurs. It is reported that these secretary granules are released following PKC activation [25–27]. It is possible that the E-64-d-mediated elimination of PKC breakdown improves the release of secretary granules.

Zheng et al. [28] reported that PKC inhibitors, H7 and staurosporin markedly suppressed the killing of *S. aureus* by monocytes, which were stimulated by cross-linking FcγR I or II. They suggested that PKC isozymes play important roles in both the stimulation and inhibition of the FcγR-mediated intracellular killing of bacteria by monocytes. Our data indicated that the PKC inhibitor, GÖ6976, blocked the bactericidal activity of PMNs against *S. aureus* at an early stage (30 min) at doses known to suppress Ca^{2+}-dependent PKC activity. We previously showed that PKCβ is autophosphorylated in the presence of ceramide, which is increased in CHS cells, and promotes the calpain-mediated proteolysis of PKCβ [29]. At the doses used in this study, GÖ6976 inhibits conventional PKC isozymes, including PKCβ. Therefore, it is likely that a decline in PKC is related to the deficiency of NK cell-mediated cytolysis or bactericidal activity observed in CHS.

The experiments using PKC inhibitors in this study may not fully explain the function of E-64-d in CHS patients. However, we previously reported that ceramide increases in cells from CHS patients and beige mice after Con A simulation [12,16], and that ceramide promotes calpain-mediated proteolysis of PKCβ [29]. In the present study, we showed that E-64-d reverses the down-regulation of PKC in PBMCs isolated from CHS patients (Fig. 2), and in addition, PKC plays important roles in NK and bactericidal activity (Fig. 3). Therefore, it was suggested that the improvement of NK and bactericidal activity by E-64-d in CHS is associated with the reversal of PKC activity.

It is known that factor associated with neutral sphingomyelinase (FAN) is structurally homologous to CHS1. Other researchers have stated that size regulation of lysosome by FAN is not coupled to an abnormal down-regulation of PKC [30]. However, they also mentioned that they cannot rule out a role of PKC in lysosomal formation in

Table 2
Effect of PKC inhibitors on the bactericidal activity of normal PMNs

Treatment	Bactericidal activity (% *S. aureus* killed)		
	30 min	60 min	90 min
Medium	41.93±0.76	65.03±1.58	90.8±1.32
Chelerythrin	34.57±1.24*	53.4±0.89*	79.77±0.87*
GÖ6976	36.26±0.59*	55.4±1.45*	80.7±0.86*

Normal PMNs were incubated with chelerythrin (2 μM) or GÖ6976 (10 nM) for 30 min. Then the bactericidal activity was examined as described in "Materials and methods". Data represent the mean±SE of three experiments.
*$p<0.01$, significant when compared with medium alone.

immune cells such as PMNs and macrophages. Significantly, we recently reported that E-64-d countered PMN dysfunction in beige mice [15]. Therefore, it is likely that in PMNs and NK cells, which contribute to host immune defense, the abnormal down-regulation of PKC may play a crucial role in the defects observed in CHS. We also recently showed that both neutral and acidic sphingomyelinase activities are enhanced after Con A stimulation in CHS cell lines [16]. The relationship between FAN and our findings, however, still remains to be elucidated.

The fact that E-64-d decreases the susceptibility to *S. aureus* infection in beige mice [15] and improves both the NK and bactericidal activities in cells isolated from CHS patients *in vitro* in our current study indicates that E-64-d may be an effective treatment to counteract infections in CHS patients.

Acknowledgement

This work was partially supported by a grant from the Taisho Pharmaceutical Company (Saitama, Japan).

References

[1] Chediak M. Nouvelle anomalie leukocytaire de caractere constitutionel et familiel. Rev Hematol 1952;7:362–7.
[2] Higashi O. Congenital gigantism of peroxidase granules. Tohoku J Exp Med 1954;59:315–32.
[3] Roder JC, Haliotis T, Klein M, Kores S, Jett JR, Ortaldo J, et al. A new immunodeficiency disorder in humans involving NK cells. Nature 1980;284:553–5.
[4] Jones KL, Stewart RM, Fowler M, Fukuda M, Holcombe RF. Chediak–Higashi lymphoblastoid cell lines: granule characteristics and expression of lysosome-associated membrane proteins. Clin Immunol Immunopathol 1992;65:219–26.
[5] Barbosa MDFS, Nguyen QA, Tchernev VT, Ashley JA, Detter JC, Blaydes SM, et al. Identification of the homologous beige and Chediak–Higashi syndrome gene. Nature 1996;382:262–5.
[6] Nagle DL, Karim MA, Woolf EA, Holmgren L, Bork P, Misumi DJ, et al. Identification and mutation analysis of the complete gene for Chediak–Higashi syndrome. Nat Genet 1996;14:307–11.
[7] Barbosa MDFS, Barrat FJ, Tchernev VT, Nguyen QA, Mishra VS, Colman SD, et al. Identification of mutations in two major mRNA isoforms of the Chediak–Higashi syndrome gene in human and mouse. Hum Mol Genet 1997;6:1091–8.
[8] Perou CM, Leslie JD, Green W, Li L, Ward DM, Kaplan J. The beige/Chediak–Higashi syndrome gene encodes a widely expressed cytosolic protein. J Biol Chem 1997;272:29790–4.
[9] Ward DM, Shiflett SL, Huynh D, Vaughn M, Prestwich G, Kaplan J, et al. Use of expression constructs to dissect the functional domains of the CHS/Beige protein: Identification of multiple phenotypes. Traffic 2003;4:403–15.
[10] Ito M, Tanabe F, Takami Y, Sato A, Shigeta S. Rapid down-regulation of protein kinase C in (Chediak–Higashi syndrome) beige mouse by phorbol ester. Biochem Biophys Res Commun 1988;153:648–56.
[11] Ito M, Sato A, Tanabe F, Ishida E, Takami Y, Shigeta S. The thiol proteinase inhibitors improve the abnormal rapid down-regulation of protein kinase C and the impaired natural killer cell activity in (Chediak–Higashi syndrome) beige mouse. Biochem Biophys Res Commun 1989;160:433–40.
[12] Tanabe F, Cui SH, Ito M. Abnormal down-regulation of PKC is responsible for giant granule formation in fibroblasts from CHS (beige) mice — a thiol proteinase inhibitor, E-64-d, prevents giant granule formation in beige fibroblasts. J Leukoc Biol 2000;67:749–55.
[13] Nishizuka Y. Studies and perspectives of protein kinase C. Science 1986;233:305–12.
[14] Sato A, Tanabe F, Ito M, Ishida E, Shigeta S. Thiol proteinase inhibitors reverse the increased protein kinase C down-regulation and concanavalin A cap formation in polymorphonuclear leukocytes from Chediak–Higashi syndrome (beige) mice. J Leukoc Biol 1990;48:377–81.
[15] Morimoto M, Tanabe F, Kasai F, Ito M. Effect of a thiol proteinase inhibitor, E-64-d, on susceptibility to infection with *Staphylococcus aureus* in Chediak–Higashi syndrome (beige) mice. Int Immunopharmacol 2007;7:973–80.
[16] Cui SH, Tanabe F, Terunuma H, Iwatani Y, Nunoi H, Agematsu K. A thiol proteinase inhibitor, E-64-d, corrects the abnormalities in concanavalin A cap formation and the lysosomal enzyme activity in leukocytes from patients with Chediak–Higashi syndrome by reversing the down-regulated protein kinase C activity. Clin Exp Immunol 2001;125:283–90.
[17] Gallin JI, Elin RJ, Hubert RT, Fauci AS, Kaliner MA, Wolff SM. Efficacy of ascorbic acid in Chediak–Higashi syndrome (CHS): studies in human and mice. Blood 1979;53:226–34.
[18] Jarvis WD, Turner AJ, Povirk LF, Traylor RS, Grant S. Induction of apoptotic DNA fragmentation and cell death in HL-60 human promyelocytic leukemia cells by pharmacological inhibitors of protein kinase C. Cancer Res 1994;54:1707–14.
[19] Martiny-Baron G, Kananietz MG, Mischak H, Blumberg PM, Kochs G, Hug H, et al. Selective inhibition of protein kinase C isozymes by the iodolocarbazole GÖ6976. J Biol Chem 1993;268:9194–7.
[20] Root RK, Rosenthal AS, Balestra DJ. Abnormal bactericidal, metabolic and lysosomal functions of Chediak–Higashi syndrome leukocytes. J Clin Invest 1972;51:649–65.
[21] Vassalli JD, Granelli-Piperno A, Griscelli G, Reich E. Specific protease deficiency in polymorphonuclear leukocytes of Chediak–Higashi syndrome and beige mice. J Exp Med 1978;22:1285–90.
[22] Lindmark A, Gullberg U, Olsson J. Processing and intracellular transport of cathepsin G and neutrophil elastase in the leukemic myeloid cell line U937 — modulation by brefeldin A, ammonium chloride, and monensin. J Leukoc Biol 1994;55:50–7.
[23] Ito M, Tanabe F, Sato A, Takami Y, Shigeta S. A potent inhibitor of protein kinase C inhibits natural killer activity. Int J Immunopharmacol 1988;10:211–6.
[24] Steele TA, Brahmi Z. Inhibition of human natural killer cell activity by the protein kinase C inhibitor 1-(5-isoquinolinesulfonyl)-2-methylpiperazine is an early but post-binding event. J Immunol 1988;141:3164–9.
[25] Liu D, Xu L, Yang F, Li D, Gong F, Xu T. Rapid biogenesis and sensitization of secretory lysosomes in NK cells mediated by target-cell recognition. Proc Natl Acad Sci USA 2005;102:123–7.
[26] Ting AT, Schoon RA, Abraham RT, Leibson PJ. Interaction of between protein kinase C-dependent and G protein-dependent pathways in the regulation of natural killer cell granule exocytosis. J Biol Chem 1992;267:23957–62.
[27] Atkinson EA, Gerrard JM, Hides GE, Greenberg AH. Studies of the mechanism of natural killer (NK) degranulation and cytotoxicity. J Leukoc Biol 1990;47:39–48.
[28] Zheng L, Zomerdijk TPL, Aarnoudse C, van Furth R, Nibbering PH. Role of protein kinase C isozymes in Fcγ receptor-mediated intracellular killing of *Staphylococcus aureus* by human monocytes. J Immunol 1995;155:776–84.
[29] Tanabe F, Cui SH, Ito M. Ceramide promotes calpain-mediated proteolysis of protein kinase Cβ in murine polymorphonuclear leukocytes. Biochem Biophys Res Commun 1998;242:129–33.
[30] Mohlig H, Mathieu S, Thon L, Frederiksen MC, Ward D, Kaplan J, et al. The WD repeat protein FAN regulates lysosome size independent from abnormal downregulation/membrane recruitment of protein kinase C. Exp Cell Res 2007;313:2703–18.

ELSEVIER

Novel Mutation of Early, Perinatal-Onset, Myopathic-Type Very-Long-Chain Acyl-CoA Dehydrogenase Deficiency

Seigo Korematsu, MD, PhD*,
Yujiro Kosugi, MD*,
Toshihide Kumamoto, MD, PhD†,
Seiji Yamaguchi, MD, PhD‡, and
Tatsuro Izumi, MD, PhD*

A male neonate demonstrated fetal distress, neonatal asphyxia, and transient hyper-creatine kinase-emia (8400IU/L), followed by repeated episodes of rhabdomyolysis 1-2 times/year during infancy and early childhood. At age 6 years, decreased levels of total and free carnitine in serum, and mild fiber size variation and increased fatty droplets in muscle, were confirmed. Both blood and serum fatty-acid analysis demonstrated elevated 5-tetradecenoate levels, and the acyl-CoA dehydrogenase activity of the palmitoyl-CoA/octanoyl-CoA ratio decreased in skin fibroblasts. The sequenced clone analysis of a complimentary DNA fragment revealed a compound heterozygote mutation of exon 9 (A790G) and exon 10 (997 ins T), which is a novel mutation of a myopathic-type very-long-chain acyl-CoA dehydrogenase deficiency. The patient has reached age 13 years. By treatment with an avoidance of fasting, feeding with a high-carbohydrate and low-fat diet, and intravenous drip infusion soon after every onset of rhabdomyolysis, his physical and mental development has stayed within the normal range. Patients with a perinatal onset of myopathic-type very-long-chain acyl-CoA dehydrogenase deficiency have not yet been reported. His novel mutation might be related to his clinical characterization.

Korematsu S, Kosugi Y, Kumamoto T, Yamaguchi S, Izumi T. Novel mutation of early, perinatal-onset, myopathic-type very-long-chain acyl-CoA dehydrogenase deficiency. Pediatr Neurol 2009;41:151-153.

Introduction

Very-long-chain acyl-CoA dehydrogenase deficiency is one of the disorders of fatty-acid β-oxidation [1,2]. It is divided into three phenotypes, i.e., early infantile-onset cardiac type, childhood-onset hypoglycemic type, and adolescent/adult-onset myopathic type [3-5].

Here, we describe a boy with perinatal-onset, myopathic–type, very-long-chain acyl-CoA dehydrogenase deficiency, with repeated episodes of rhabdomyolysis during infancy and early childhood, and a novel compound-heterozygote missense mutation.

Case Report

The patient is the second child of nonconsanguineous, healthy Japanese parents. He demonstrated sudden fetal distress just after the beginning of his mother's labor at 41 weeks of gestation, and was born by vaginal delivery. His Apgar score was 5 at 1 minute. His laboratory findings at birth revealed an elevated serum level of creatine kinase of 8400 IU/L, alanine aminotransferase of 155 IU/L, and asparatate aminotransferase of 16 IU/L. His blood glucose level was 56 mg/dL. After mask and bagging resuscitation and intravenous drip infusion, his physical condition and creatine kinase elevation improved within a few days.

Thereafter, his psychomotor and growth development has been normal. He was able to walk alone and began to speak at age 12 months. He exhibited repeated episodes of rhabdomyolysis with hyper-CK-emia at 20,000-50,000 IU/L, which was usually triggered by a common cold and hard physical exercise 3-4 times/year during infancy and early childhood (Table 1). Neither cardiomyopathy nor hypoglycemia was evident.

At age 6 years, because his serum levels of both total and free carnitine were decreased (18.8 μmol/L (normal range: 45-91) and 15.7 μmol/L (normal range: 36-74), respectively), a muscle biopsy from his left biceps was performed. A muscle biopsy revealed fiber-size variations, with an atrophy of type 2B fibers (Fig 1a). However, no grouped atrophy, necrotic and degenerating fibers, ragged red fibers, rimmed vacuoles, or nemaline bodies were evident. On oil red-O staining, many fatty-acid deposits were evident (Fig 1b).

A fatty-acid analysis [6], using dried-blood filter paper and serum analysis, indicated elevated 5-tetradecenoate levels of 39.6 μM (normal range; not detected) and 55.8 μM (not detected), respectively. The acyl-CoA dehydrogenase activity with octanoyl-CoA was 4.71 μM (normal range:

From the *Department of Pediatrics and Child Neurology, and †Department of Neurology and Neuromuscular Disorders, Faculty of Medicine, Oita University, Oita, Japan, and ‡Department of Pediatrics, Shimane University Faculty of Medicine, Shimane, Japan.

Communications should be addressed to:
Dr. Korematsu; Department of Pediatrics and Child Neurology; Faculty of Medicine, Oita University; Hasama, Yufu, Oita 879-5593, Japan.
E-mail: kseigo@med.oita-u.ac.jp
Received September 24, 2008; accepted February 23, 2009.

doi:10.1016/j.pediatrneurol.2009.02.020 • 0887-8994/09/$—see front matter

Table 1. Lab data of a 6-year old male patient with VLCAD deficiency during rhabdomyolysis

Complete blood count		Serum chemistry		Blood gas analysis		Serum fatty acid analysis		Acyl-CoA dehydrogenase activity	
WBC	2900/μl	AST	1,640 IU/l	pH	7.451	Serum		Skin fibroblast	
RBC	441 × 10^4/μl	ALT	480 IU/l	pCO_2	37.8 mmHg	C_8	4.3 μmol/l (4.8-9.2)	CS	31.8 (41.0-68.3)
Hb	12.5 g/dl	CK	46,000 IU/l	HCO_3^-	25.7 mmol/l	C_{10}	10.6 μmol/l (4.2-7.8)	C_4	2.17 (1.38-2.50)
Ht	35.0%	LDH	573 IU/l	BE	1.9 mmol/l	$C_{10:1}$	0 μmol/l (n.d.)	C_8	4.71 (3.64-5.06)
PLT	15.0 × 10^4/μl	ALP	537 IU/l			$C_{14:1}$	55.8 μmol/l (n.d.)	C_{16}	0.87 (2.42-5.06)
		γGTP	11 IU/l					C_{16}/C_8	0.18 (0.63-0.68)
		Glucose	108 mg/dl						
		Aldolase	16.5 IU/l						
		Lactate	15.7 mg/dl						
		Total-carnitine	19.7 μmol/l (45-91)						
		Free-carnitine	15.4 μmol/l (36-74)						
		Acyl-carnitine	4.3 μmol/l (6-23)						

Abbreviations:
C_4: Butyryl-CoA
C_8: Octanoyl-CoA
C_{16}: Palmitoyl-CoA
C_{10}: Decenoate
$C_{10:1}$: 4-decenoate
$C_{14:1}$: 5-tetradecenoate
CS: Citrate synthetase

3.64-5.06), and that with palmitoyl-CoA was 0.87 μM (normal range: 2.42-5.06), in skin fibroblasts. The ratio of palmitoyl-CoA/octanoyl-CoA decreased to 0.18 (normal range: 0.63-0.68). Moreover, a sequenced clone analysis of the complimentary DNA fragment revealed a compound heterozygote mutation of exon 9, i.e., A790 G (K264E), and exon of 10, i.e., 997 ins T (frameshift).

The patient is presently aged 13 years and 4 months. Through treatment with an avoidance of fasting, feeding with a high-carbohydrate and low-fat diet, and intravenous drip infusion soon after every onset of rhabdomyolysis, his physical and mental development has stayed within normal range. His body weight and height are 47.0 kg (−0.1 S.D.) and 165.4 cm (+1.0 S.D.), respectively.

Discussion

A boy with myopathic-type very-long-chain acyl-CoA dehydrogenase deficiency experienced repeated episodes of rhabdomyolysis since the perinatal period. His gene analysis revealed a novel compound-heterozygote mutation of exon 9, i.e., A790 G (K264E), and exon 10, i.e., 997 ins T (frameshift).

Mitochondrial β-oxidation of fatty acid is an important source of energy for metabolic processes, including normal fasting, muscular activity, and illness. Moreover, very-long-chain acyl-CoA dehydrogenase deficiency is one of the disorders of mitochondrial β-oxidation of fatty acid [1,2]. Very-long-chain acyl-CoA dehydrogenase deficiency is divided into three phenotypes [3-5]. The cardiac type is a severe form that involves hypertrophic cardiomyopathy and sometimes leads to sudden death in the early infantile period. The hypoglycemic type is of moderate-severity

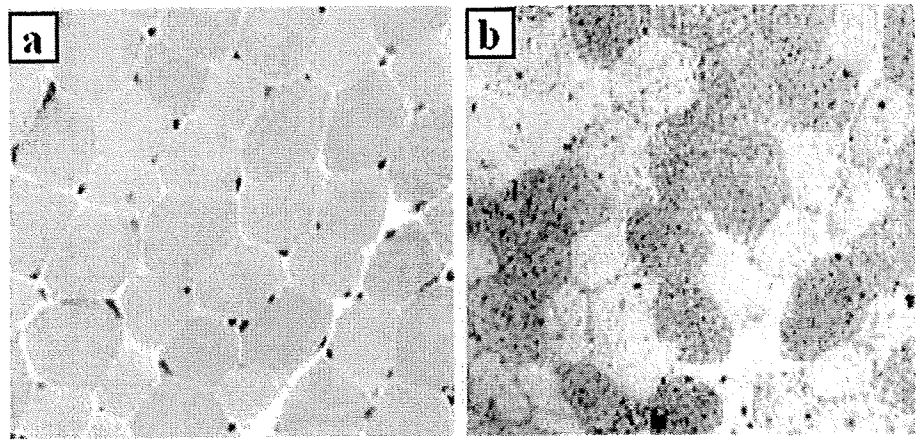

Figure 1. Muscle histochemical findings. a: Hematoxylin-eosin stain (original magnification ×400). b: Oil red-O stain (original magnification ×400). There were fiber-size variations. Small fibers were of type 2B, and type-1 fibers were predominant. A small number of basophilic fibers were evident. No grouped atrophy, small angular fibers, myophagia, glycogen storage, necrotic and degenerating fibers, ragged red fibers, rimmed vacuoles, or nemaline bodies were evident. On oil red-O staining, many fatty-acid deposits were evident.

childhood onset, with repeated hypoglycemia. The myopathic type of this disease is of mild severity and adolescent or adult onset, with intermittent rhabdomyolysis.

Roe et al. [7] found that the residual enzyme activity of the palmitoyl-CoA/octanoyl-CoA ratio is closely correlated with these phenotypes. The cardiac type exhibited a severe decrease to 0.025 ± 0.028 S.D., whereas both the hypoglycemic and the myopathic types demonstrated a moderate decrease, to 0.058 ± 0.058 S.D. Moreover, these phenotypes are delineated in terms of their gene mutation [8]. Cardiac-type patients were shown to manifest "null"or homozygous mutations, whereas hypoglycemia-type and myopathic-type patients tend to manifest missense mutations, including compound heterozygosity.

Because of repeated rhabdomyolysis, and the findings of acyl-CoA dehydrogenase activity and a heterozygote missense mutation, our patient was diagnosed with myopathic-type very-long-chain acyl-CoA dehydrogenase deficiency. Neonatal onset was reported in patients with the cardiac and hypoglycemic types [3-5,9], but not in patients with the myopathic type. Ito et al. [10] reported on a 9-month-old infant who had been the youngest patient to date with the myopathic type. The clinical characterization and onset of very-long-chain acyl-CoA dehydrogenase deficiency may therefore involve a broad spectrum. This novel gene mutation might be related to the patient's early, perinatal onset and his repeated rhabdomyolysis. We need the accumulation of such findings to evaluate a distinct relationship.

We thank Yuki Hasegawa, MD (Department of Pediatrics, Shimane University) for fatty-acid gene analysis.

References

[1] **Yamaguchi** S, Indo Y, Coates PM, Hashimoto T, Tanaka K. Identification of very long chain acyl-CoA dehydrogenase deficiency in three patients previously diagnosed with long-chain acyl-CoA dehydrogenase deficiency. Pediatr Res 1993;34:111-3.

[2] **Aoyama** T, Uchida Y, Kelly RI, et al. A novel disease with deficiency of mitochondrial very-long-chain acyl-CoA dehydrogenase. Biochem Biophys Res Commun 1993;191:1369-72.

[3] **Vianey-Saban** C, Divry P, Brivet M, et al. Mitochondrial very-long-chain acyl-coenzyme A dehydrogenase deficiency: Clinical characteristics and diagnostic considerations in 30 patients. Clin Chim Acta 1998;269:43-62.

[4] **Strauss** AW, Powell CK, Hale DE, et al. Molecular basis of human mitochondrial very-long-chain acyl-CoA dehydrogenase deficiency causing cardiomyopathy and sudden death in childhood. Proc Natl Acad Sci USA 1995;92:10496-500.

[5] **Souri** M, Aoyama T, Orii K, Yamaguchi S, Hashimoto T. Mutation analysis of very-long-chain acyl-coenzyme A dehydrogenase (VLCAD) deficiency: Identification and characterization of mutant VLCAD cDNAs from four patients. Am J Hum Genet 1996;58:97-106.

[6] **Kimura** M, Yoon HR, Wasant P, Takahashi Y, Yamaguchi S. A sensitive and simplified method to analyze free fatty acids in children with mitochondrial beta oxidation disorders using gas chromatography/mass spectrometry and dried blood spots. Clin Chim Acta 2002;316:117-21.

[7] **Roe** DS, Vianey-Saban C, Sharma S, Zabot MT, Roe CR. Oxidation of unsaturated fatty acids by human fibroblasts with very-long-chain acyl-CoA dehydrogenase deficiency: Aspects of substrate specificity and correlation with clinical phenotype. Clin Chim Acta 2001;312:55-67.

[8] **Andresen** BS, Olpin S, Poortuis BJ, et al. Clear correlation of genotype with disease phenotype in very-long-chain acyl-CoA dehydrogenase deficiency. Am J Hum Genet 1998;64:479-94.

[9] **Aliefendioglu** D, Dursun A, Coskun T, Akcoren Z, Wanders RJ, Waterham HR. A newborn with VLCAD deficiency. Clinical, biochemical, and histopathological findings. Eur J Pediatr 2007;166:1077-80.

[10] **Ito** Y, Nakano K, Shishikura K, et al. A two-year-old infant with a myopathic form of very-long-chain acyl-CoA dehydrogenase deficiency. No To Hattatsu 2003;35:491-7.

ABSTRACT: Previous studies have documented the presence of rimmed vacuoles, atrophic fibers, and increased lysosomal cathepsin activity in skeletal muscle from animal models of chloroquine-induced myopathy, suggesting that muscle fibers in this type of myopathy may be degraded via the lysosomal-proteolysis pathway. Given recent evidence of abnormal ubiquitin accumulation in rimmed vacuoles, in this study we chose to examine the significance of the ubiquitin–proteasome proteolytic system in the process of muscle fiber destruction in experimental chloroquine myopathy. Expression of ubiquitin, 26S proteasome proteins, and ubiquitin ligases, such as muscle-specific RING finger-1 (MuRF-1) and atrogin-1/muscle atrophy F-box protein (MAFbx), was analyzed in innervated and denervated rat soleus muscles after treatment with either saline or chloroquine. Abnormal accumulation of rimmed vacuoles was observed only in chloroquine-treated denervated muscles. Ubiquitin and proteasome immunostaining, and ubiquitin, MuRF-1, and atrogin-1/MAFbx mRNAs were significantly increased in denervated soleus muscles from saline- and chloroquine-treated rats when compared with contralateral innervated muscles. Further, ubiquitin and ubiquitin ligase mRNA levels were higher in denervated muscles from chloroquine-treated rats when compared with saline-treated rats. These data demonstrate increased proteasomes and ubiquitin in denervated muscles from chloroquine-treated rats and suggest that the ubiquitin–proteasome proteolysis pathway as well as the lysosomal-proteolysis pathway mediate muscle fiber destruction in experimental chloroquine myopathy.
Muscle Nerve **39:** 521–528, 2009

ROLE OF UBIQUITIN–PROTEASOME PROTEOLYSIS IN MUSCLE FIBER DESTRUCTION IN EXPERIMENTAL CHLOROQUINE-INDUCED MYOPATHY

NORIYUKI KIMURA, MD, TOSHIHIDE KUMAMOTO, MD, TAKAHIRO ONIKI, MD, MIWA NOMURA, MD, KENICHIRO NAKAMURA, MD, YOSHITAKE ABE, MD, YUSUKE HAZAMA, MD, and HIDETSUGU UEYAMA, MD

Department of Neurology and Neuromuscular Disorders, Faculty of Medicine, Oita University, Idaigaoka 1-1, Hasama, Yufu, Oita 879-5593, Japan

Accepted 8 October 2008

The autophagic-lysosome system plays an important role in the degradation and turnover of intracellular proteins and organelles in skeletal muscles.[5] Chloroquine, a lysosomotropic agent, mediates autophagic protein degradation in the autophagic-lysosome system and promotes accumulation of sequestered materials in the autophagosome by terminating protein degradation in the lysosome system. Indeed, chloroquine-treated muscle displays rimmed vacuoles of dense granular bodies and vacuoles, which include variably sized and shaped autophagosomes.[11,20]

The rimmed vacuole is the pathological hallmark of chloroquine myopathy in humans and animals. Given the frequency of rimmed vacuoles in various myopathies, such as distal myopathy with rimmed vacuoles (DMRV) and inclusion-body myopathy (IBM), it is important to gain an understanding of the mechanisms and regulation involved in their formation. We previously demonstrated that denervation induces marked accumulation of rimmed vacuoles in experimental chloroquine-induced myopathy, although in human chloroquine myopathy there may be not such a condition, except for incidental denervation, such as with compression radiculopathy due to spondylosis. Specifically, we ob-

Abbreviations: ATP, adenosine triphosphate; MuRF-1, muscle-specific RING finger-1; MAFbx, muscle atrophy F-box protein; DMRV, distal myopathy with rimmed vacuoles; RT-PCR, semiquantitative reverse transcriptase–polymerase chain reaction; IgG, immunoglobulin G; cDNA, complementary DNA; GAPDH, glyceraldehyde-3-phosphate dehydrogenase; IBM, inclusion-body myopathy; IGF-1, insulin-like growth factor-1

Key words: atrogin-1/MAFbx; chloroquine; denervation; MuRF-1; rimmed vacuoles; ubiquitin

Correspondence to: T. Kumamoto; e-mail: kumagoro@med.oita-u.ac.jp

Published online 15 March 2009 in Wiley InterScience (www.interscience.wiley.com). DOI 10.1002/mus.21223

served an increased number of rimmed vacuoles and severe atrophic fibers in denervated chloroquine-treated rat muscles as well as the absence of these findings in contralateral, innervated chloroquine-treated muscle and in the innervated muscles of saline-treated rats.[13] Further, immunostaining for cathepsins B and L (lysosomal protease) was increased in denervated muscle from chloroquine-treated rats, suggesting that progression of the degenerative process in this myopathy is mediated by the lysosomal-autophagic process.[13] Because both an autophagic-lysosomal process and a non-lysosomal process (i.e., calpain and ubiquitin–proteasome proteolytic pathways)[15,22] mediate degradation of muscle fibers in denervated muscles,[12] chloroquine-induced dysfunction of the autophagic-lysosome process could represent an excellent mechanistic explanation for vacuole formation.[13]

In DMRV and IBM, rimmed vacuoles and some vacuole-free fibers contain abnormally high amounts of ubiquitin,[1,12] which modifies cellular proteins and targets abnormal or normal proteins for highly selective breakdown by an adenosine triphosphate (ATP)-dependent pathway.[10,16] Recent evidence has indicated that the non-lysosomal ATP–ubiquitin-dependent proteolytic protease, as a multicatalytic protease complex (proteasome), can meditate muscle wasting in the context of various catabolic states.[10,16,23] Degradation of a protein via this pathway involves two distinct steps. The first is signaling by the covalent attachment of multiple ubiquitin molecules. This is followed by degradation of the targeted protein by an ATP-dependent protease, the 26S (1500 kDa) proteasome,[23] with the subsequent release of free, reutilizable ubiquitin. The proteasome is found in both the cytoplasm and the nucleus of muscle cells and may be responsible for muscle fiber degradation.[2,9,10,15] Further, the ATP–ubiquitin-dependent proteolytic pathway is responsible for the bulk of muscle protein breakdown, including that of myofibrillar proteins (e.g., myosin and actin) during various physiological and pathological conditions (e.g., starvation, denervation, metabolic acidosis, and sepsis).[2,9,10,15]

Proteins degraded by the ubiquitin–proteasome proteolytic pathway are first conjugated to multiple molecules of ubiquitin.[6,9,10,17] This reaction requires the activation of ubiquitin by the ubiquitin-activating enzyme (E1), transfer to a ubiquitin-conjugating enzyme (E2), and subsequent linkage to the lysine residue in proteins destined for degradation. The latter reaction is catalyzed by the ubiquitin ligases (E3).[6,9,10,17] This series of reactions is repeated until the target protein is labeled with a polyubiquitin chain. The polyubiquitin-conjugated proteins are recognized by the 19S subunit of the proteasome, and they are subsequently degraded into peptides in the 20S proteasome core. Among these enzymes, different members of the E2 and ubiquitin ligase families work in concert and account for substrate and tissue specificity.[9,10] Recent studies have suggest that, in addition to E3α, other ubiquitin ligases, including muscle-specific RING finger-1 (MuRF-1) and atrogin-1/muscle atrophy F-box protein (MAFbx), may regulate muscle protein breakdown in various catabolic conditions and may actually be more important than E3α for the development of muscle wasting.[3,14,17,24] In fact, these ubiquitin ligases are increased in skeletal muscle atrophy induced by nutrient deprivation, unloading, diabetes, uremia, and cancer.[3,14,17] Bodine et al. reported that gene expression of the ubiquitin ligases MuRF-1 and MAFbx was substantially upregulated in rat skeletal muscle after institution of conditions that are all associated with a significant loss of muscle mass,[24] including immobilization, denervation, hindlimb suspension, or treatment with interleukin-1 or dexamethasone.[3]

Although the influence of certain catabolic conditions on the expression of MuRF-1 and atrogin-1/MAFbx in skeletal muscles has been reported previously,[17,24] expression of these genes in skeletal muscles from chloroquine-induced myopathy is not known. Thus, the goal of this study was to characterize the significance of the ubiquitin–protease-dependent proteolytic pathway in muscle fiber destruction by conducting immunohistochemical and real-time reverse transcriptase–polymerase chain reaction (RT-PCR) studies on the innervated and denervated skeletal muscles from saline- and chloroquine-treated rats.

METHODS

Animals. The left hindlegs of 40 adult male Wistar rats (200–250 g) were denervated by ligation of the sciatic nerve, as previously described.[13] Chloroquine chloride (50 mg/kg body weight) was injected intraperitoneally into 20 rats twice daily, beginning on the day after denervation. The remaining 20 rats received saline injections. The soleus muscles from the right (innervated) and left (denervated) legs were obtained from the chloroquine- and saline-treated rats on days 4, 8, and 16 after the initial injection. The muscles were rapidly frozen in isopentane cooled in liquid nitrogen.

Histologic and Immunohistochemical Studies. Routine histologic analysis was performed using cryostat sections (10-μm thick), as described previously.[12,13] Hematoxylin–eosin preparations of each specimen were analyzed with an image analyzer (Cosmozon ISA; Nikon, Tokyo, Japan) attached to a Macintosh computer (Apple, Cupertino, California). The number of fibers with dense granular bodies or vacuoles at the light-microscopic level were determined from 400 muscle fibers per muscle.

For immunofluorescence analysis, frozen tissue sections were fixed in 4% paraformaldehyde for 20 min. For antigen retrieval, sections were immersed in 10 mM sodium citrate buffer, pH 6.0 (Iatron, Tokyo, Japan), autoclaved at 120°C for 10 min, and cooled to room temperature. Unstained sections were incubated overnight at 4°C with a monoclonal antibody for the 20S proteasomes (diluted 1:50; Santa Cruz Biotechnology, Santa Cruz, California) or for ubiquitin (diluted 1:200; Chemicon International, Temecula, California). After washing, Alexa Fluor 488–labeled goat anti-mouse immunoglobulin G (IgG; H+L) (diluted 1:250; Molecular Probes, Eugene, Oregon) was added for 1 h. Specimens were mounted on slides for visualization by fluorescence microscopy. Images were captured using a confocal laser scanning microscope (LSM5 Pasal-V3.2; Carl Zeiss, Oberkochen, Germany).

Immunostaining was specific, because there was no staining when sections were allowed to react without the first-layer antibodies or when normal goat serum was substituted for the antibody.

Real-Time RT-PCR. Innervated and denervated soleus muscles from saline- and chloroquine-treated rats were excised, frozen rapidly in liquid nitrogen, and stored at −80°C until use. Total RNA was isolated from specimens using acid guanidinium thiocyanate buffer (Nippon Gene, Tokyo, Japan), according to the manufacturer's instructions. The purity of the RNA was checked by the ratio of absorbance at 260 and 280 nm. Complementary DNA (cDNA) was synthesized from 1 μg of total RNA using 200 units of Moloney murine leukemia virus reverse transcriptase (Gibco BRL, Rockville, Maryland) and 1 μg of oligo-(dT)12–18 primer (Invitrogen, Tokyo, Japan). Gene-specific primers for real-time PCR were purchased from Takara Bio, Inc. (Otsu, Shiga, Japan). The nucleotide sequences of the primers used in this study were as follows: rat MuRF-1 mRNA (Accession No. NM 080903; sense, 5′-GGG AAC GAC CGA G TT CAG ACT ATC-3′; antisense, 5′-GGC GTC AAA CTT GTG GCT CA-3′), rat atrogin-1/MAFbx 32 mRNA (Accession No. NM 133521; sense, 5′-AGT GAA G AC CGG CTA CTG TGG AA-3′; antisense, 5′-TTG CAA AGC TGC AGG GTG AC-3′), rat ubiquitin-C mRNA (Accession No. NM 017314; sense, 5′-GGG CAT GCA GAT CTT TGT GAA-3′; antisense, 5′-ACC TCC AGG GTG ATG GTC TTG-3′), and rat glyceraldehyde-3-phosphate dehydrogenase (GAPDH) mRNA (Accession No. NM 017008; sense, 5′-GAC AAC TTT GGC ATC GTG GA-3′; antisense, 5′-ATG CAG GGA TGA TGT TCT GG-3′). Quantitative real-time RT-PCR was performed using a LightCycler 2.0 instrument (Roche Diagnostics, Mannheim, Germany) and version 4.0 software, respectively. The reaction mixture consisted of 1:25 diluted cDNA (5 μl), 0.2 μM of each primer, 2 μl of LightCycler FastStart DNA Master SYBR-Green I mix (Roche Diagnostics), and 4 mM of $MgCl_2$ in a total volume of 20 μl. The PCR conditions consisted of one denaturing cycle at 95°C for 10 min, followed by 45 cycles consisting of denaturing at 95°C for 10 s, annealing at 55°C for 10 s, and extension at 72°C for 10 s. Formation of expected PCR product was confirmed by agarose gel electrophoresis (2%) and melting curve analysis. The relative amount of mRNA expression was calculated by measuring the threshold cycle of each PCR product compared with the GAPDH mRNA as an internal control. All PCR runs were performed in triplicate.

Statistical Analysis. Differences between control specimens and disease specimens were evaluated with the unpaired t-test. $P < 0.05$ was considered statistically significant.

RESULTS

Histologic and Immunohistochemical Studies. Histologic findings for the innervated and denervated soleus muscles from saline- and chloroquine-treated rats on each test day were consistent with those from previous reports (Fig. 1).[13] Briefly, on days 4, 8, and 16 after the initial injection, the majority of the right innervated soleus muscles of the saline and chloroquine-treated rats appeared to be normal. By contrast, the left denervated muscles of both groups showed marked neurogenic changes with varying degrees of severity, as described elsewhere.[13] These muscles showed moderate or severe muscle fiber atrophy. Marked accumulations of dense granular bodies or vacuoles were observed in the denervated chloroquine-treated muscles, particularly on days 8 and 16, whereas they were very rare in the denervated saline-treated muscles.

Quantitative analysis showed that the mean diameters of the fibers in the denervated muscles of the

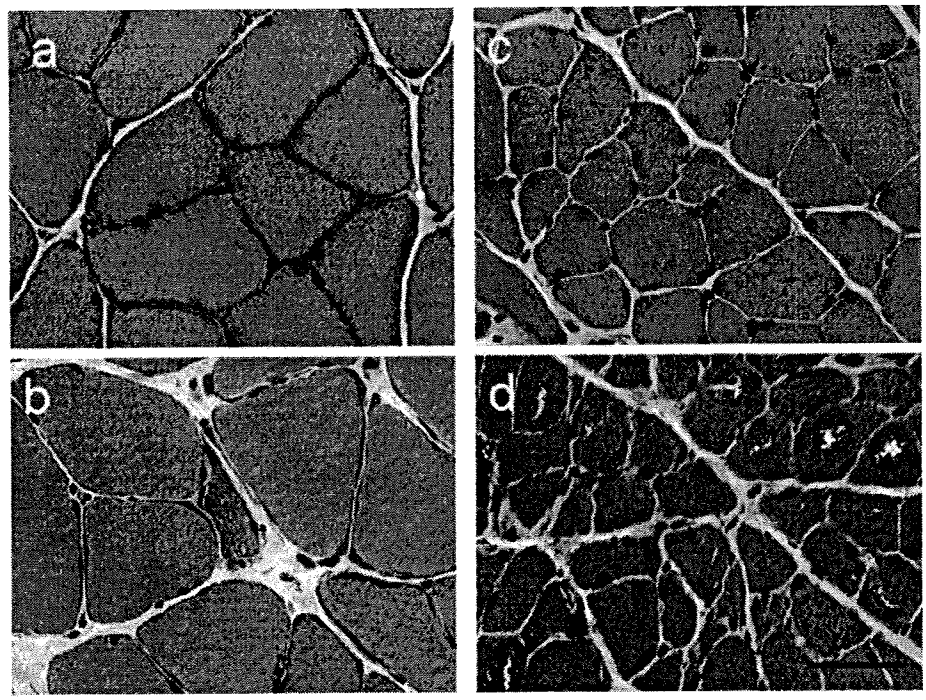

FIGURE 1. Cross-sections of rat soleus muscles after 16 days of saline or chloroquine treatment. The left denervated muscle of a saline-treated rat **(c)** compared with a chloroquine-treated rat **(d)** shows moderate muscle fiber atrophy. Many dense granular bodies and vacuoles (arrowhead) are present in the denervated muscle from chloroquine-treated rats **(d)** but are absent in denervated muscles from saline-treated rats **(c)** and innervated muscles from saline-treated **(a)** and chloroquine-treated **(b)** rats. Hematoxylin–eosin (H&E) stain. Bar = 50 μm.

saline- and chloroquine-treated rats on day 16 (32.2 ± 7.4 μm and 21.9 ± 6.4 μm, respectively) were significantly smaller than those of the innervated muscles (49.7 ± 11.2 μm and 49.5 ± 10.0 μm, respectively; $P < 0.01$). Furthermore, the mean diameter of muscle fibers in the denervated muscles of chloroquine-treated rats was significantly smaller than that of saline-treated rats ($P < 0.001$). By contrast, the diameters did not differ significantly in comparison with innervated muscles of the experimental animal groups.

Immunostaining for 20S proteasomes and ubiquitin was minimal in innervated muscles from saline- and chloroquine-treated rats at all time-points, whereas denervated muscles from both groups showed progressively stronger staining for these proteins with increasing time (Fig. 2). Strong positive reaction for proteasomes and ubiquitin was often observed in the cytoplasm, primarily in small atrophic fibers and within vacuoles in the denervated muscles of chloroquine-treated rats. The qualitative immunohistochemical analysis showed that the denervated muscles of chloroquine-treated rats had strong positive reactions when compared with saline-treated rats. Increased ubiquitin-positive granules were observed in the sarcoplasm, especially in muscle fibers containing vacuoles and occasionally in the vacuoles themselves.

Ubiquitin and Ubiquitin Ligase mRNA Levels. Ubiquitin, MuRF-1, and atrogin-1/MAFbx mRNA levels were measured in the innervated and denervated soleus muscles of saline- and chloroquine-treated rats at various time-points (Figs. 3–5). Ubiquitin mRNA levels were unchanged in all experimental muscles on day 4 when compared with innervated muscles from saline-treated rats on day 4 after initial injection. Elevation in ubiquitin mRNA levels occurred on days 8 and 16 in denervated muscles from chloroquine-treated rats (7.3- and 4.5-fold increased relative to innervated muscle from saline-treated rats on days 8 and 16, respectively; on day 8, $P < 0.05$; on day 16, $P < 0.02$). Ubiquitin mRNA levels in denervated muscles from saline-treated rats increased 2.6-fold (on day 8, $P < 0.02$) and 1.3-fold (on day 16, P = not significant [NS]) than those of innervated muscles from saline-treated rats on days 8 and 16, respectively. Ubiquitin mRNA levels in the denervated muscles of chloroquine-treated rats tended to be higher than in saline-treated rats on days 8 and 16

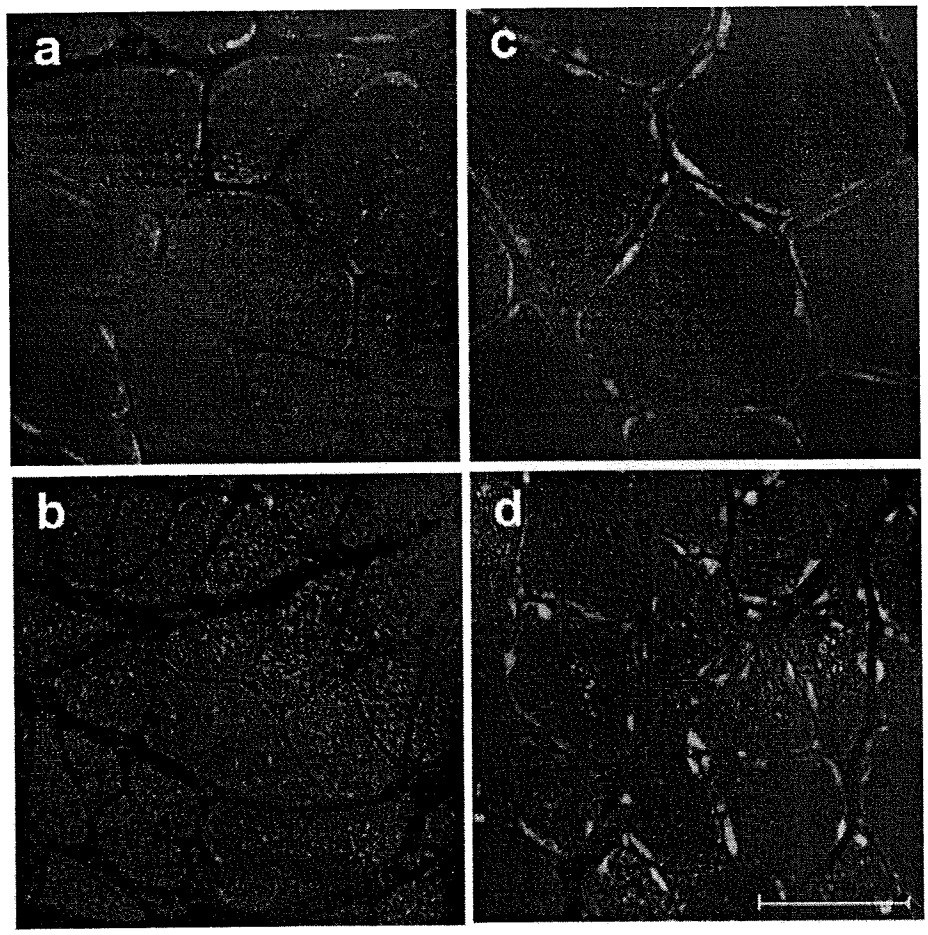

FIGURE 2. Immunofluoresence for anti-20S proteasome **(a, b)** and anti-ubiquitin **(c, d)** antibodies in innervated and denervated rat soleus muscles after 16 days of chloroquine treatment. A strong positive reaction for proteasome **(b)** and ubiquitin **(d)** is often observed in the cytoplasm, primarily in small atrophic fibers, and within the vacuoles in the denervated muscles of chloroquine-treated rats. Bar = 50 μm.

(on day 8, P = NS; on day 16, $P < 0.05$). Innervated muscles from chloroquine-treated rats were essentially similar when compared with innervated muscles from saline-treated rats on each test day (Fig. 3).

MuRF-1 mRNA levels in denervated muscles of saline-treated rats subsequently increased from day 4, peaked on day 8, and then decreased to the control levels on day 16. The mRNA levels in these muscles were 2.3-fold (on day 4, $P < 0.05$), 3.3-fold (on day 8, $P < 0.01$), and 1.2-fold (on day 16, P = NS) higher than those of innervated muscles from saline-treated rats on days 4, 8, and 16, respectively (Fig. 4). MuRF-1 mRNA levels were increased in the denervated muscles from chloroquine-treated rats on all test days. Levels on days 4, 8, and 16 were 2.9-, 2.1-, and 2.4-fold those of innervated muscles from saline-treated rats, respectively (on day 4, $P < 0.02$; on day 8, $P < 0.05$; on day 16, P = NS).

In the denervated muscles from saline-treated rats, atrogin-1/MAFbx mRNA levels abruptly increased to 7.1-fold ($P < 0.01$) those of innervated muscles from saline-treated rats on day 8 and then returned to the control muscle value on day 16. Atrogin-1/MAFbx mRNA levels in denervated muscles from chloroquine-treated rats subsequently increased from day 4 and peaked on day 16. Atrogin-1/MAFbx mRNA levels in these muscles were 2.8-, 3.7-, and 5.6-fold those of involved muscles from saline-treated rats on days 4, 8, and 16, respectively (on day 4, $P < 0.01$; on day 8, $P < 0.01$; on day 16, $P < 0.05$) (Fig. 5). MuRF-1 and atrogin-1/MAFbx mRNA levels in denervated muscles from chloroquine-treated rats were lower on day 8 and higher on day 16 compared with saline-treated animals, but the differences were not statistically significant.

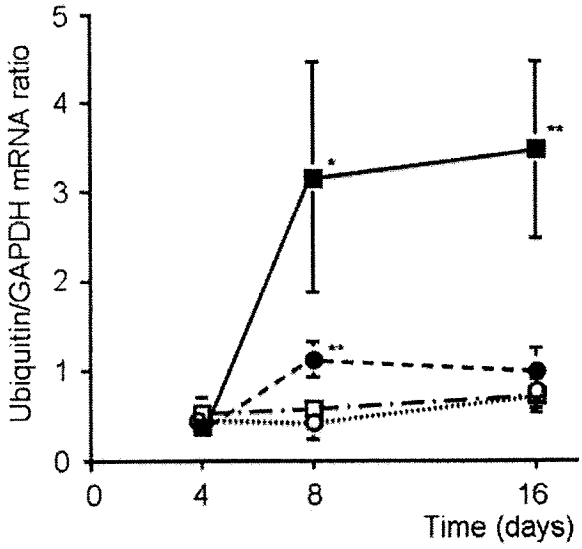

FIGURE 3. (a) Changes in ubiquitin mRNA levels in innervated and denervated rat soleus muscles on days 4, 8, and 16 of saline or chloroquine treatment. Points represent mean ± standard deviation (vertical lines). Number of rats per group = 5. (○) Innervated muscle from saline-treated rats; (●) denervated muscles from saline-treated rats; (□) innervated muscle from chloroquine-treated rats; (■) denervated muscle from chloroquine-treated rats. $^{*}P < 0.05$; $^{**}P < 0.02$; $^{***}p < 0.01$ vs. the value for innervated muscle from saline-treated rats.

DISCUSSION

This study has demonstrated an increase in the dense granular bodies and vacuoles (primarily autophagosomes and, a lesser extent, autolysosomes) in denervated soleus muscles from chloroquine-treated rats, which is consistent with previous reports.[13] An increase in vacuole formation was observed as early as day 2, with progressive increases thereafter. In particular, chloroquine-treated denervated muscle showed severe fiber atrophy and some necrosis as well as dense granular bodies and vacuoles. Our previous electron microscopy study revealed streaming of the Z-disk, loss of normal muscle filaments, and disruption of the normal banding patterns, in denervated muscles from chloroquine-treated rats, representing muscle fiber destruction.[13]

Like other tissues, muscle has at least three different pathways for protein breakdown: proteolytic by lysosomal proteases (e.g., cathepsins); proteolysis by non-lysosomal, intracellular Ca^{2+}-dependent proteases (e.g., calpain); and proteolysis by non-lysosomal, ATP–ubiquitin-dependent proteolytic proteases, which function as multicatalytic protease complexes (proteasomes).[7,16,23] Proteolysis by lysosomal cathepsins and by the calpain pathway is thought to cause muscle fiber destruction in the innervated and denervated muscles from saline- and chloroquine-treated rats. However, their intracellular distribution and role have not been studied in diseased muscles, including muscle affected by denervation and chloroquine treatment. In this study, immunohistochemical investigation has revealed that proteasomes were present in the cytoplasm of innervated muscle from saline- and chloroquine-treated rats, although the staining intensity was very weak. By contrast, in denervated muscle specimens from chloroquine-treated rats, proteasomes were moderately to strongly expressed in atrophic and necrotic fibers, and staining activity increased during subsequent experimental days. Moreover, denervated muscles from saline-treated rats showed mild positive immunostaining for proteasomes. On qualitative immunohistochemical analysis, this staining activity tended to be stronger in denervated muscles from chloroquine-treated rats than in saline-treated rats. Immunoreactivity for ubiquitin was occasionally positive in the cytoplasm of these atrophic fibers. Therefore, the increased staining for proteasome in atrophic fibers may be the result of upregulation of proteasome expression, which suggests that the ubiquitin–proteasome proteolytic pathway may be

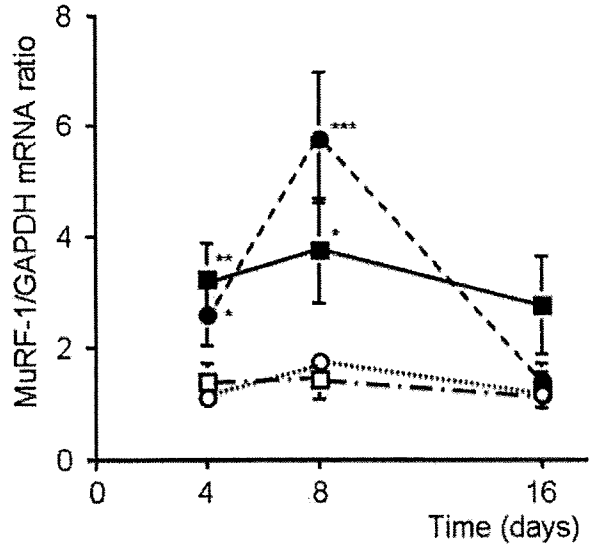

FIGURE 4. Changes in MuRF-1 mRNA levels in innervated and denervated soleus muscles on days 4, 8, and 16 of saline and chloroquine treatment. Points represent mean ± standard deviation (vertical lines). Number of rats per group = 5. (○) Innervated muscle from saline-treated rats; (●) denervated muscle from saline-treated rats; (□) innervated muscle from chloroquine-treated rats; (■) denervated muscle from chloroquine-treated rats. $^{*}P < 0.05$; $^{**}P < 0.02$; $^{***}p < 0.01$ vs. the value for innervated muscle from saline-treated rats.

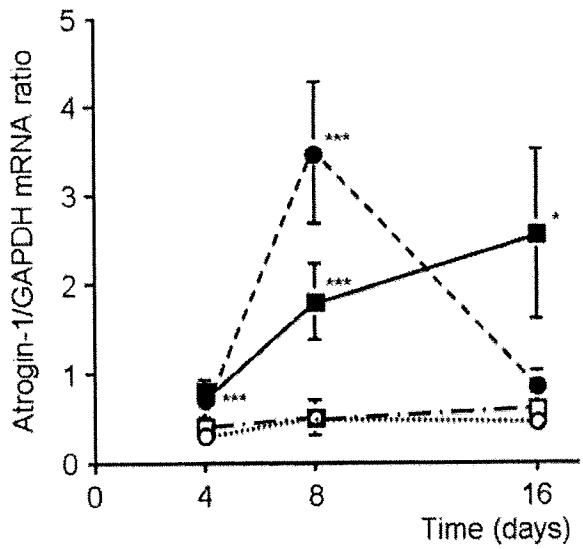

FIGURE 5. Changes in atrogin-1/MAFbx mRNA in innervated and denervated rat soleus muscles on days 4, 8, and 16 of saline or chloroquine treatment. Points represent mean ± standard deviation (vertical lines). Number of rats per group = 5. (O) Innervated muscles from saline-treated rats; (●) denervated muscles from saline-treated rats; (squ;) innervated muscle from chloroquine-treated rats; (squf;) denervated muscle from chloroquine-treated rats. $^{*}p < 0.05$; $^{**}p < 0.02$; $^{***}p < 0.01$ vs. the value for innervated muscle from saline-treated rats

responsible for muscle fiber destruction of denervated muscles, especially in chloroquine-treated rats.

The MuRF-1 and atrogin-1/MAFbx-expressing genes are only present in muscle tissues; this may be an indication that these ubiquitin ligases are muscle-specific. MuRF-1 is probably bound to the Z-disk by heterodimerization with MuRF-3.[19] MuRF-1 is speculated to play a role in the ubiquitination and degradation of titin and perhaps other proteins in the Z-disk, resulting in disruption of the Z-disk and release of actin and myosin.[24] Atrogin-1/MAFbx specifically regulates protein breakdown in skeletal muscles under the catabolic condition of denervation, immobilization, treatment with interleukin-1 or dexamethasone, sepsis, fasting, and renal failure.[3,7,24] In the present study, we found that gene expression of newly described ubiquitin ligases, MuRF-1 and atrogin-1/MAFbx, is significantly increased in the denervated soleus muscles of saline- and chloroquine-treated rats when compared with that of the innervated muscles from both groups. This result may indicate that expression of ubiquitin ligase proteins, such as MuRF-1 and atrogin-1/MAFbx, is increased by denervation treatment alone and has a specific role in myofibrillar protein degradation in the denervated muscles of saline- and chloroquine-treated rats.

This study has demonstrated that the mRNA levels of MuRF-1 and atrogin-1/MAFbx were significantly increased on day 8 in denervated muscles of saline- and chloroquine-treated rats relative to those in innervated muscles from saline-treated rats. These levels tended to be higher in denervated saline-treated rats than in denervated chloroquine-treated animals, although the difference was not statistically significant. This result suggests that, in rats, the abrupt elevation of ubiquitin ligase mRNA levels may be slightly decreased during an earlier stage of muscle fiber degradation by denervation as compared with denervation alone because of the slow degradation rate or turnover of intracellular proteins, lipids, glycogen, and organelles via the autophagic-lysosomal system with chloroquine treatment. However, on day 16, mRNA levels in the denervated muscles of saline-treated rats decreased to the same level as that in innervated saline-treated muscles, whereas levels in denervated muscles from chloroquine-treated rats remained unchanged. This result suggests that, over the 7 days after initial ligation of the sciatic nerve, denervation induced progressive muscle atrophy, resulting in a marked increase in mRNA levels of muscle-specific ubiquitin ligase molecules. Because axonal sprouting (i.e., reinnervation) is a rapid process that is completed within 2 weeks after partial denervation of rat soleus muscle,[21] the decrease of these mRNA levels in the denervated muscles of saline-treated rats on day 16 may be due to the end of denervation-induced muscle fiber degradation.

The mRNA levels of ubiquitin, MuRF-1, and atrogin-1/MAFbx were increased to a greater extent in denervated muscles from chloroquine-treated rats when compared with those from saline-treated rats on day 16, although reinnervation occurred in the chloroquine group. The simplest interpretation of these findings is that chloroquine-muscle atrophy is still progressing, even on day 16. Therefore, chloroquine treatment promotes activation of ubiquitin, MuRF-1, and atrogin-1/MAFbx, and their upregulation may enhance the ubiquitin–proteasome proteolytic pathway, with subsequent induction of muscle fiber destruction in the denervated soleus muscle from chloroquine-treated rats.

In this study we have demonstrated that ubiquitin mRNA levels increased in denervated muscles from chloroquine-treated rats, but it remained the same in denervated muscles from saline-treated rats. Immunohistochemical analysis for ubiquitin confirmed this difference; staining activity was stronger in the denervated muscles from chloroquine-treated rats when compared with saline-treated rats. The mech-

anism underlying this difference in ubiquitin expression remains unclear.

In conclusion, these data suggest that skeletal muscle atrophy and muscle fiber destruction occur through increased activity of the ubiquitin–proteasome proteolytic pathways in chloroquine-treated muscle after denervation. Recent studies have demonstrated that insulin-like growth factor-1 (IGF-1) stimulates muscle protein synthesis and hypertrophy via the phosphatidylinositol-3-kinase–Akt pathway, and activation of this pathway can reduce muscle atrophy.[4,18] IGF-1 rapidly suppresses atrogin-1 and polyubiquitin expression and also suppresses MuRF-1.[1] Therefore, it would be beneficial to determine whether IGF-1 can suppress muscle fiber atrophy and destruction in this myopathy.

The authors thank Y. Umeki, K. Sato, M. Ono, and K. Hirano for technical assistance.

REFERENCES

1. Askanas V, Engel WK, Mirabella M. Idiopathic inflammatory myopathies: inclusion-body myositis, polymyositis, and dermatomyositis. Curr Opin Neurol 1994;7:448–456.
2. Beyette JR, Mykles DL. Immunocytochemical localization of the multicatalytic proteinase (proteasome) in crustacean striated muscles. Muscle Nerve 1992;15:1023–1035.
3. Bodine SC, Latres E, Baumhueter S, Lai VK, Nunez L, Clarke BA, et al. Identification of ubiquitin ligases required for skeletal muscle atrophy. Science 2001;294:1704–1708.
4. Bodine SC, Stitt TN, Gonzalez M, Kline WO, Stover GL, Bauerlein R, et al. Akt/mTOR pathway is a crucial regulator of skeletal muscle hypertrophy and can prevent muscle atrophy in vivo. Nat Cell Biol 2001;3:1014–1019.
5. Gerard KW, Hipkiss AR, Schneider DL. Degradation of intracellular protein in muscle. Lysosomal response to modified proteins and chloroquine. J Biol Chem 1988;263:18886–18890.
6. Glickman MH, Ciechanover A. The ubiquitin–proteasome proteolytic pathway: destruction for the sake of construction. Physiol Rev 2002;82:373–428.
7. Goll DE, Kleese WC, Kumamoto T, Cong J, Szpacenko A. In search of the regulation and function of the Ca^{2+}-dependent proteinases (calpain). In: Katunuma N, Kominami E, editors. Intracellular proteolysis, mechanism and regulation. Tokyo: Japanese Scientific Societies Press; 1989. p 82–91.
8. Gomes MD, Lecker SH, Jagoe RT, Navon A, Goldberg AL. Atrogin-1, a muscle-specific F-box protein highly expressed during muscle atrophy. Proc Natl Acad Sci USA 2001;98: 14440–14445.
9. Hasselgren PO, Fischer JE. The ubiquitin–proteasome pathway: review of a novel intracellular mechanism of muscle protein breakdown during sepsis and other catabolic conditions. Ann Surg 1997;225:307–316.
10. Hershko A, Ciechanover A. The ubiquitin system. Annu Rev Biochem 1998;67:425–479.
11. Kumamoto T, Araki S, Watanabe S, Ikebe N, Fukuhara N. Experimental chloroquine myopathy: morphological and biochemical studies. Eur Neurol 1989;29:202–207.
12. Kumamoto T, Fujimoto S, Nagao S, Masuda T, Sugihara R, Ueyama H, et al. Proteasomes in distal myopathy with rimmed vacuoles. Intern Med 1998;37:746–752.
13. Kumamoto T, Ueyama H, Watanabe S, Murakami T, Araki S. Effect of denervation on overdevelopment of chloroquine-induced autophagic vacuoles in skeletal muscles. Muscle Nerve 1993;16:819–826.
14. Lecker SH, Jagoe RT, Gilbert A, Gomes M, Baracos V, Bailey J, et al. Multiple types of skeletal muscle atrophy involve a common program of changes in gene expression. FASEB J 2004;18:39–51.
15. Medina R, Wing SS, Goldberg AL. Increase in levels of polyubiquitin and proteasome mRNA in skeletal muscle during starvation and denervation atrophy. Biochem J 1995;307:631–637.
16. Mitch WE, Goldberg AL. Mechanisms of muscle wasting. The role of the ubiquitin–proteasome pathway. N Engl J Med 1996;335:1897–1905.
17. Razeghi P, Baskin KK, Sharma S, Young ME, Stepkowski S, Essop MF, et al. Atrophy, hypertrophy, and hypoxemia induce transcriptional regulators of the ubiquitin proteasome system in the rat heart. Biochem Biophys Res Commun 2006;342: 361–364.
18. Sacheck JM, Ohtsuka A, McLary SC, Goldberg AL. IGF-I stimulates muscle growth by suppressing protein breakdown and expression of atrophy-related ubiquitin ligases, atrogin-1 and MuRF1. Am J Physiol Endocrinol Metab 2004;287:E591–E601.
19. Spencer JA, Eliazer S, Ilaria RL Jr, Richardson JA, Olson EN. Regulation of microtubule dynamics and myogenic differentiation by MURF, a striated muscle RING-finger protein. J Cell Biol 2000;150:771–784.
20. Stauber WT, Hedge AM, Trout JJ, Schottelius BA. Inhibition of lysosomal function in red and white skeletal muscles by chloroquine. Exp Neurol 1981;71:295–306.
21. Thompson W, Jansen JK. The extent of sprouting of remaining motor units in partly denervated immature and adult rat soleus muscle. Neuroscience 1977;2:523–535.
22. Ueyama H, Kumamoto T, Fujimoto S, Murakami T, Tsuda T. Expression of three calpain isoform genes in human skeletal muscles. J Neurol Sci 1998;155:163–169.
23. Voisin L, Breuille D, Combaret L, Pouyet C, Taillandier D, Aurousseau E, et al. Muscle wasting in a rat model of long-lasting sepsis results from the activation of lysosomal, Ca^{2+}-activated, and ubiquitin–proteasome proteolytic pathways. J Clin Invest 1996;97:1610–1617.
24. Wray CJ, Mammen JM, Hershko DD, Hasselgren PO. Sepsis upregulates the gene expression of multiple ubiquitin ligases in skeletal muscle. Int J Biochem Cell Biol 2003 ;35:698–705.

Archives of Gerontology and Geriatrics 49 (2009) 322–325

Contents lists available at ScienceDirect

Archives of Gerontology and Geriatrics

journal homepage: www.elsevier.com/locate/archger

Influence of age on symptoms and laboratory findings at presentation in patients with influenza-associated pneumonia

Osamu Matsuno [a,b,*], Hajime Kataoka [c], Ryuichi Takenaka [b,d], Fumiko Okubo [b,d], Kenjiro Okamoto [d], Kazuhiro Masutomo [d], Yoichiro Hiramoto [d], Eishi Miyazaki [b], Toshihide Kumamoto [b]

[a] Division of Respiratory Disease, Osaka Minami Medical Center, Kidohigashimachi 2-1, Kawachinagano city, Osaka 586-8521, Japan
[b] Division of Respiratory Disease and Neurology, Third Department of Internal Medicine, Oita University Faculty of Medicine, Idaigaoka 1-1, Hasama-machi, Yufu city, Oita 879-5593, Japan
[c] Department of Internal Medicine, Nishida Hospital, Saiki-city, Oita 876-0831, Japan
[d] Division of Internal Medicine, Usuki Cosmos Hospital, Nagaya 1131-1, Usuki city, Oita 876-0051, Japan

ARTICLE INFO

Article history:
Received 29 May 2008
Received in revised form 14 November 2008
Accepted 17 November 2008
Available online 15 January 2009

Keywords:
Influenza complications in elderly
Influenza-related pneumonia
C-reactive protein
Neuraminidase inhibitor therapy

ABSTRACT

Influenza virus infection is a major respiratory infectious disease that generally induces pneumonia. The clinical manifestations of influenza virus infection and community-acquired pneumonia (CAP) differ between elderly persons and younger adults. To determine the clinical features of influenza-associated pneumonia, we studied 21 adult patients with influenza-associated pneumonia, as indicated by positive test results for influenza virus antigen. At presentation, the higher-age patients (≥75 years; $n = 12$) with influenza-associated pneumonia had lower body temperature than did the lower-age (<75 years) patients ($n = 9$). Conversely, the laboratory data indicated significantly higher C-reactive protein (CRP) concentration in higher-age patients than that in lower-age patients. None of the 18 patients undergoing neuraminidase inhibitor therapy died, but two of three patients who did not receive this therapy died from complications of advanced pneumonia. In this study, vaccination did not appear to be an important factor for prevention of pneumonia. High-age patients with CAP have lower body temperature, raising the possibility that diagnosis and treatment may be delayed in these patients. Increased CRP levels in these patients at presentation, however, could contribute to early detection of this serious pulmonary complication.

1. Introduction

Studies of community-acquired pneumonia (CAP) in adults indicate a viral etiology in 1–23% of cases, with influenza virus being the most common agent (File, 2003). Pure viral pneumonia is uncommon among older patients (Falsey and Walsh, 2006). Viral infections, however, may predispose patients to bacterial disease (Potter, 1998). Subsequent development of secondary bacterial pneumonia following influenza is a leading cause of mortality worldwide. Although distinguishing viral from bacterial causes on the basis of clinical findings is difficult, epidemiologic and clinical clues can be helpful in alerting physicians to the possibility of viral pneumonia. Recently, the diagnosis of influenza has become easy and accurate due to the development of a rapid antigen detection kit.

The clinical manifestations of influenza may differ between elderly persons and younger adults, with older persons having a lower frequency of signs of upper respiratory tract dysfunction (Govaert et al., 1998). The older people (≥75 years) had also a 15-fold higher incidence of CAP associated with influenza virus than young adults (Gutiérrez et al., 2006). Fever and altered mental status is reported to be the only sign of influenza-associated pneumonia in older patients (Walsh et al., 2002).

Systemic data regarding the clinical picture of patients developing serious complication of influenza-associated pneumonia are few. A new class of therapeutic agents (neuraminidase = NA-inhibitors) was recently approved for use in patients with influenza. Thus, in the present study we examined the clinical features of influenza-associated pneumonia and the benefits of vaccination and use of newly developed antiviral agents for treatment of the disease.

* Corresponding author at: Division of Respiratory Disease and Neurology, Third Department of Internal Medicine, Oita University Faculty of Medicine, Idaigaoka 1-1, Hasama-machi, Yufu city, Oita 879-5593, Japan. Tel.: +81 97 586 5814; fax: +81 97 549 6502.
E-mail addresses: matsuno@med.oita-u.ac.jp, matsuno@ommc-hp.jp (O. Matsuno).

0167-4943/$ – see front matter © 2008 Elsevier Ireland Ltd. All rights reserved.
doi:10.1016/j.archger.2008.11.015

Table 1
Clinical characteristics of 21 patients with influenza-associated pneumonia.

Case no.	Sex/age year	Underlying disease	Vaccination status	Influenza type	Antiviral treatment		TP (°C)	WBC	CRP	Location of pneumonia	CT findings	Sputum findings	Outcomes
					drug	interval							
Lower-age patients (<75 year) (n = 9)													
1	M/27	None	–	A	Oseltamivir	1d	39.8	11,900	6.32	RLL	CO	–	Alive
2	M/30	None	–	A	Zanamivir	1d	40.1	16,600	0.64	Bilateral	GGO, pleuritis	–	Alive
3	M/41	Sinusitis	+	A	Oseltamivir	1d	38.6	11,800	13.93	Bilateral	Inf, CO	Negative	Alive
4	F/41	Leukopenia	–	B	Oseltamivir	0d	37.1	2,800	0.4	Bilateral	Inf, CO	Negative	Alive
5	M/43	Epilepsy MR	+	A	Oseltamivir	0d	39 8	20,500	11 48	LUL LLL	Inf, GGO		Alive
6	F/49	MR	+	A	Oseltamivir	1d	40	1600	10.66	Bilateral	Inf	*H. influenza*	Alive
7	M/67	DM, hepatitis	–	A	Oseltamivir	3d	38.3	4,000	1.02	Bilateral	Inf	Negative	Alive
8	M/72	None	–	A	Oseltamivir	0d	38.2	6500	1.68	Bilateral	BP	Negative	Alive
9	M/74	CVD, GC	+	A	Oseltamivir	4d	38.1	7,600	16.22	Bilateral	Inf	–	Alive
High-age patients (≥75 year) (n = 12)													
10	M/76	CVD, CHF	+	B	Oseltamivir	2d	38.2	12,300	9.54	RLL	Inf	*P. aeruginosa*	Alive
11	M/77	EC, Old Tb	–	B	Oseltamivir	1d	37.5	6,800	27.56	Bilateral	Inf, GGO, Effusion	Negative	Alive
12	F/77	Old Tb	Unknown	A	Amantadine	2d	37.3	7,000	5.47	Bilateral	Inf, GGO	MRSA	Dead
13	F/80	OC	–	B	Oseltamivir	0d	37.2	10,000	44.54	Bilateral	BP, GGO	Negative	Alive
14	M/82	None	–	A	Oseltamivir	0d	37.8	14,000	22.4	Bilateral	Inf	*S. pneumoniae*	Alive
15	F/82	Tighbone fracture, BC	Unknown	A	Oseltamivir	0d	36.9	6,800	2.57	Bilateral	Inf	MRSA	Alive
16	F/84	Asthma	–	A	None	–	36.6	4,000	21.98	Bilateral	GGO	Negative	Alive
17	F/84	None	–	B	Oseltamivir	3d	36.7	4,400	4.59	Bilateral	BP, Effusion	MSSA	Alive
18	F/85	None	+	A	Oseltamivir	5d	38.6	10,800	12.59	RLL	BOOP	*S. pneumoniae*	Alive
19	F/87	CHF	–	A	None	–	37.4	5,800	18.36	RLL	Inf	*P. aeruginosa*	Dead
20	M/87	CVD	+	B	Oseltamivir	0d	36.7	8,400	3.97	Bilateral	Inf, Effusion	Negative	Alive
21	F/89	CVD	–	A	Oseltamivir	CPd	38.3	5,800	19.65	Bilateral	Inf	MSSA	Alive

CVD; cerebral vascular desease, MR; mental retardation, CHF; congestive heart failure, BC; breast cancer, DM; diabetes mellitus, OC; ovarian cancer, EC; esophageal cancer, Tb; tuberculosis, GC; gastric cancer, LUL; left upper lung, LLL; left lower lung, RLL; right lowere lung, Inf; infiltration, GGO; ground glass opacity, BP; bronchopneumonia, CO; centrilobular opacity.

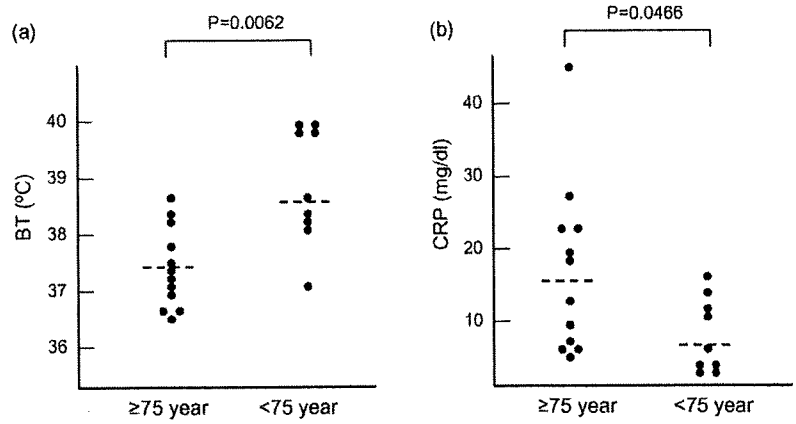

Fig. 1. (a) Body temperature (BT) in higher-age and lower-age patients. (b) Serum CRP levels in higher and lower-age patients. Significant differences are shown on the top.

2. Methods

2.1. Subjects and diagnostic criteria

The study population was composed of hospitalized patients from three hospital-based study sites (Oita University Hospital, Cosmos Hospital, and Nishida Hospital). Louria et al. (1959) classified pulmonary complications of influenza into four categories: no radiographic pneumonia, viral infection followed by bacterial pneumonia, rapidly progressive diffuse viral infection, and concomitant viral-bacterial pneumonia. In this study, influenza-associated pneumonia was strictly defined by the existence of newly-appearing pulmonary infiltrate(s) on thoracic radiograph. Only data for subjects with such radiograph findings were included in the analysis. Twenty-one patients with influenza-associated pneumonia admitted to the hospitals from December 2003 to March 2007 were included in the study. Influenza virus infection was confirmed using a rapid antigen detection kit (Espline Influenza A and B-N; Fujirebo, Tokyo, Japan) and nasopharyngeal swab specimens. Sputum sampling by semi-quantitative bacterial culturing was performed for the study patients (except for patients who did not have non-productive cough).

2.2. Statistical analysis

Patient clinical data were not normally distributed and were statistically analyzed using nonparametric statistics: the Mann–Whitney U test. A $p < 0.05$ was considered statistically significant.

3. Results

Characteristics of the 21 study patients are summarized in Table 1. Among 20 patients with known influenza vaccination data, 7 were vaccinated during the previous fall seasons. None of the patients had received antibiotics prior to hospital admission. At presentation with influenza-associated pneumonia, higher-age patients (≥75 years; $n = 12$) had a significantly lower body temperature, compared with the lower-age patients (<75 years; $n = 9$; Fig. 1a). The laboratory data also indicated significantly higher C-reactive protein (CRP) levels in high-age, compared with lower-age patients (Fig. 1b). On thoracic computed tomography, bilateral diffuse interstitial/alveolar infiltrates were the most common abnormal findings (76.2%), followed by right lower lung lobe consolidation (19%). Centrolobular opacity was an exceptional finding, observed in only three lower-age patients. Vaccination status, male to female ratio, and influenza type did not affect clinical and laboratory findings.

Respiratory tract bacterial culture results were positive in 9 of 17 patients who underwent the procedure. *Staphylococcus aureus* ($n = 4$), followed by Streptococcus pneumoniae ($n = 2$), were the most frequently isolated pathogens. Of the four patients positive for *S. aureus*, two had methicillin-resistant strains.

Antiviral agents were administered to 19 of the 21 (90.5%) patients, with Oseltamivir (81.0%) used most frequently. From day 1 of hospital admission, all patients were treated with broad-spectrum medicines. In all patients, antiviral medication was administered for a total of 5 days and was well tolerated. None of the 18 patients given the NA-inhibitor died. Two of the three patients not treated with the NA-inhibitor, however, died from complications of advanced pneumonia, even though one of these patients was treated with amantadine. One of the two patients that died of pneumonia had not been vaccinated during the previous fall season.

4. Discussion

The most important findings from this study are: compared with lower-age (<75 years) patients, high-age (≥75 years) patients with influenza-associated pneumonia have a significantly lower body temperature and higher CRP levels.

Advanced age has become a well-recognized risk factor for death in patients with pneumonia (Louria et al., 1959; Marrie et al., 1989; Fine et al., 1990). Older patients with CAP have less severe symptoms such as cough, sputum and fever, raising the possibility that diagnosis and treatment of this disease may be delayed in these patients (Fine et al., 1995). In elderly outpatients with influenza-associated upper respiratory tract infection, cough, fever, and acute onset of illness had only 30% positive predictive value, in contrast to 78% positive predictive value for similar symptoms in young patients (Metlay et al., 1997). The results of our study support those previous observations: fever was less common among high-age patients with influenza-associated pneumonia. Elderly patients with influenza-associated pneumonia might present with more attenuated symptoms, but this should not be misconstructed as an indication that such patients are less severely affected.

Though symptomatic detection of influenza-associated pneumonia in high-age patients might often be difficult, increased CRP levels in these patients at presentation could contribute to early detection of this serious pulmonary complication. Almirall et al. (2004) reported that serum CRP level is a useful marker for establishing the diagnosis of CAP in adult patients with lower respiratory tract infection. To our knowledge, there are no previous reports of a comparison between older and younger patients with

influenza-associated pneumonia. The results of our study indicate that high-age patients present with higher CRP levels than lower-age patients. CAP has more serious clinical and abnormal laboratory features in the elderly than younger patients, particularly in those over 75 (Lieberman et al., 1997). One explanation for the great increase in CRP levels in higher-age patients is that lower fever in these patients might be reflected by an increasing tendency toward delayed diagnosis, leading to the progression of pulmonary inflammation and higher CRP levels at presentation. Whatever the cause of the increase in CRP levels, measurement of this serum component is a simple method for evaluating higher-age patients that are suspected of having influenza-associated pneumonia.

The benefits of the use of antiviral agents for treatment of influenza-associated pneumonia are unknown, because to our knowledge, placebo-controlled trials for pneumonia have not been conducted (Oliveria et al., 2001; Falsey and Walsh, 2006). Due to the small sample size and the uncontrolled nature of our study, the impact of the NA-inhibitor on the outcome of influenza-associated pneumonia could not be determined; however, none of the patients treated with NA-inhibitors died. In the past, treatment options have been limited to amantadine and rimantadine (an inhibitor of the ion-channel activity of the M2 protein), but more recently two new NA-inhibitors (inhaled zanamivir and orally administered oseltamivir (an inhibitor specific for influenza-virus NA), were approved for use. The efficacy of these new antiviral agents in human patients with influenza-associated pneumonia, however, is unknown.

With regard to the influenza vaccination, much controversy surrounds its role in the prevention of hospitalization for influenza and/or pneumonia (Nordin et al., 2001; Hak et al., 2002; Voordouw et al., 2003; McCullers, 2004; Hara et al., 2006; Skull et al., 2007). Further studies are required to address these questions.

Conflict of interest

None.

References

Almirall, J., Bolíbar, I., Toran, P., Pera, G., Boquet, X., Balanzó, X., Sauca, G., 2004. Contribution of C-reactive protein to the diagnosis and assessment of severity of community-acquired pneumonia. Chest 125, 1335–1342.

Falsey, A.R., Walsh, E.E., 2006. Viral pneumonia in older adults. Céin. Infect. Dis. 42, 518–524.

File, T.M., 2003. Community-acquired pneumonia. Lancet 362, 1991–2002.

Fine, M.J., Orloff, J.J., Arisumi, D., Fang, G.D., Arena, V.C., Hanusa, B.H., Yu, V.L., Singer, D.E., Kapoor, W.N., 1990. Prognosis of patients hospitalized with community-acquired pneumonia. Am. J. Med. 88, 1N–8N.

Fine, M.J., Hanusa, B.H., Lave, J.R., Singer, D.E., Stone, R.A., Weissfeld, L.A., Coley, C.M., Marrie, T.J., Kapoor, W.N., 1995. Comparison of a disease-specific and a generic severity of illness measure for patients with community-acquired pneumonia. J. Gen. Intern. Med. 10, 359–368.

Govaert, T.M.E., Dinant, G.J., Aretz, K., Knottnerus, J.A., 1998. The predictive value of influenza symptomatology in elderly people. Fam. Pract. 15, 16–22.

Gutiérrez, F., Masiá, M., Mirete, C., Soldán, B., Rodríguez, J.C., Padilla, S., Hernández, I., Royo, G., Martin-Hidalgo, A., 2006. The influence of age and gender on the population-based incidence of community-acquired pneumonia caused by different microbial pathogens. Infect 53, 166–174.

Hak, E., Nordin, J., Wei, F., Mullooly, J., Poblete, S., Strikas, R., Nichol, K.L., 2002. Influence of high-risk medical conditions on the effectiveness of influenza vaccination among elderly members of 3 large managed-care organizations. Clin. Infect. Dis. 35, 370–377.

Hara, M., Sakamoto, T., Tanaka, K., 2006. Effectiveness of influenza vaccination in preventing influenza-like illness among community-dwelling elderly: population-based cohort study in Japan. Vaccine 24, 5546–5551.

Lieberman, D., Schlaeffer, F., Porath, A., 1997. Community-acquired pneumonia in old age: a prospective study of 91 patients admitted from home. Age Ageing 26, 69–75.

Louria, D.E., Blumenfeld, H.L., Ellis, J.T., Kilbourne, E.D., Rogers, D.E., 1959. Studies on influenza in the pandemic of 1957-1958 II Pulmonary complications of influenza. J. Clin. Invest. 38, 213–265.

Marrie, T.J., Durant, H., Yates, L., 1989. Community-acquired pneumonia requiring hospitalization: 5-year prospective study. Rev. Infect. Dis. 11, 586–599.

McCullers, J.A., 2004. Effect of antiviral treatment on the outcome of secondary bacterial pneumonia after influenza. J. Infect. Dis. 190, 519–526.

Metlay, J.P., Schulz, R., Li, Y.H., Singer, D.E., Marrie, T.J., Coley, C.M., Hough, L.J., Obrosky, D.S., Kapoor, W.N., Fine, M.J., 1997. Influence of age on symptoms at presentation in patients with community-acquired pneumonia. Arch. Intern. Med. 57, 1453–1459.

Nordin, J., Mullooly, J., Poblete, S., Strikas, R., Petrucci, R., Wei, F., Rush, B., Safir-stein, B., Wheeler, D., Nichol, K.L., 2001. Influenza vaccine effectiveness in preventing hospitalizations and deaths in persons 65 years or older in Minnesota, New York, and Oregon: data from 3 health plans. J. Infect. Dis. 184, 665–670.

Oliveria, E.C., Marik, P., Colice, G., 2001. Influenza pneumonia: a descriptive study. Chest 119, 1717–1723.

Potter, C.W., 1998. Chronicle of Influenza Pandemics. Textbook of Influenza. Blackwell Scientific Publications, London.

Skull, S.A., Andrews, R.M., Byrnes, G.B., Kelly, H.A., Nolan, T.M., Brown, G.V., Campbell, D.A., 2007. Prevention of community-acquired pneumonia among a cohort of hospitalized elderly: benefit due to influenza and pneumococcal vaccination not demonstrated. Vaccine 25, 4631–4640.

Voordouw, B.C.G., Van der Linden, P.D., Simonian, S., Van der Lei, J., Sturkenboom, M., Stricker, B.H.C., 2003. Influenza vaccination in community dwelling elderly: impact on mortality and influenza-associated morbidity. Arch. Intern. Med. 163, 1089–1094.

Walsh, E.E., Cox, C., Falsey, A.R., 2002. Clinical features of influenza A virus infection in elderly hospitalized persons. J. Am. Geriatr. Soc. 50, 1498–14503.

Journal of the Neurological Sciences 281 (2009) 93–98

Contents lists available at ScienceDirect

Journal of the Neurological Sciences

journal homepage: www.elsevier.com/locate/jns

Evaluation of the effect of thyrotropin releasing hormone (TRH) on regional cerebral blood flow in spinocerebellar degeneration using 3DSRT

Noriyuki Kimura *, Toshihide Kumamoto, Teruaki Masuda, Yuki Nomura, Takuya Hanaoka, Yusuke Hazama, Toshio Okazaki, Ryuki Arakawa

Department of Internal Medicine III, Oita University, Faculty of Medicine, Idaigaoka 1-1, Hasama, Yufu, Oita 879-5593, Japan

ARTICLE INFO

Article history:
Received 14 October 2008
Received in revised form 31 December 2008
Accepted 26 January 2009
Available online 14 March 2009

Keywords:
Thyrotropin releasing hormone
Spinocerebellar degeneration
Brain perfusion SPECT
3DSRT
eZIS

ABSTRACT

Thyrotropin releasing hormone (TRH) therapy improves cerebellar ataxia in patients with spinocerebellar degeneration (SCD). We investigated the effect of TRH on regional cerebral blood flow (rCBF) using the fully automated region of interest (ROI) technique, 3DSRT. Ten patients with SCD received TRH intravenously (2 mg/day) for 14 days and underwent brain perfusion single photon emission computed tomography before and after therapy. Clinical efficacy was assessed using the International Cooperative Ataxia Rating Scale (ICARS). The rCBF in each ROI was measured using the noninvasive Patlak plot method and calculated using 3DSRT. TRH significantly improved the ICARS scores and increased rCBF in the callosomarginal segment and cerebellum. Cerebellar rCBF increased in 4 of 5 patients with improved ICARS scores and in 3 of 5 patients without improved ICARS scores after TRH therapy. The correlation between the change in cerebellar rCBF and the improved ICARS score, however, was not significant. These findings indicate that TRH therapy may increase cerebellar rCBF in some patients with cerebellar forms of SCD and that 3DSRT may be useful for evaluating the efficacy of TRH for increasing CBF. The beneficial effects of TRH may be due to increased cerebellar rCBF or the increased rCBF may be a secondary effect of TRH therapy.

1. Introduction

Thyrotropin releasing hormone (TRH) regulates the release of thyrotropin from the pituitary gland. TRH also has neuroprotective effects as a neuromodulator or neurotransmitter in the brain [1], and is therefore often used as a therapeutic agent in cases of encephalitis, trauma [2,3], brain ischemia [4], and neurodegenerative disorders [5,6]. TRH administered intravenously at a dose of 2 mg/day for 14 days significantly improves cerebellar ataxia in patients with spinocerebellar degeneration (SCD) [7,8]. Evaluation of the efficacy of TRH therapy based on clinical parameters is difficult because the degree of clinical improvement is slight and depends on the disease severity. Although brain perfusion single photon emission computed tomography (SPECT) has been used to evaluate cerebral function and to measure regional cerebral blood flow (rCBF) quantitatively using manual settings to determine the region of interest (ROI), both the reproducibility and objectivity of the results are problematic because the ROIs on the SPECT referential slice must be set equally for every patient [3,9]. Brain perfusion analyzing programs, such as eZIS and 3DSRT, were recently developed to address these problems. The eZIS program allows for the detection of significantly decreased blood perfusion in cerebral regions [10,11] and the 3DSRT program allows for the objective assessment of rCBF by automatically setting the ROIs based on anatomically standardized SPECT images [12,13]. In the present study, rCBF in 12 different brain regions was measured using the noninvasive Patlak plot method and calculated using 3DSRT both before and after 14 days of TRH therapy in SCD patients. The aim of our study was to objectively determine the efficacy of TRH therapy and to discuss the potential mechanisms underlying TRH-induced improvement of cerebellar ataxia.

2. Materials and methods

2.1. Subjects

Patients with SCD who were admitted to the Department of Neurology and Neuromuscular disorders, Oita University Hospital, for TRH therapy between January 2006 and September 2008 were included in the study. TRH therapy was administered to all patients with pure cerebellar ataxia, because TRH is particularly effective in patients with cerebellar forms of SCD [14]. Although 11 patients provided informed consent to participate in the study, 1 patient was excluded because quantitative SPECT data could not be obtained. Therefore, 10 subjects were included in the study (6 men, 4 women; age range, 52–69 years; mean age, 60.8), including 5 patients with

* Corresponding author. Tel.: +81 97 586 5814; fax: +81 97 586 6502.
E-mail address: noriyuki@med.oita-u.ac.jp (N. Kimura).

0022-510X/$ – see front matter © 2009 Elsevier B.V. All rights reserved.
doi:10.1016/j.jns.2009.01.023